JCI The Journal of Clinical Investigation

Functional polycystin-1 dosage governs autosomal dominant polycystic kidney disease severity

Katharina Hopp, … , Vicente E. Torres, Peter C. Harris

J Clin Invest. 2012;122(11):4257-4273. https://doi.org/10.1172/JCI64313.

Research Article

Autosomal dominant polycystic kidney disease (ADPKD) is caused by mutations to *PKD1* or *PKD2*, triggering progressive cystogenesis and typically leading to end-stage renal disease in midlife. The phenotypic spectrum, however, ranges from in utero onset to adequate renal function at old age. Recent patient data suggest that the disease is dosage dependent, where incompletely penetrant alleles influence disease severity. Here, we have developed a knockin mouse model matching a likely disease variant, *PKD1* p.R3277C (RC), and have proved that its functionally hypomorphic nature modifies the ADPKD phenotype. While $Pkd1^{+/null}$ mice are normal, $Pkd1^{RC/null}$ mice have rapidly progressive disease, and $Pkd1^{RC/RC}$ animals develop gradual cystogenesis. These models effectively mimic the pathophysiological features of in utero–onset and typical ADPKD, respectively, correlating the level of functional *Pkd1* product with disease severity, highlighting the dosage dependence of cystogenesis. Additionally, molecular analyses identified p.R3277C as a temperature-sensitive folding/trafficking mutant, and length defects in collecting duct primary cilia, the organelle central to PKD pathogenesis, were clearly detected for the first time to our knowledge in PKD1. Altogether, this study highlights the role that in trans variants at the disease locus can play in phenotypic modification of dominant diseases and provides a truly orthologous PKD1 model, optimal for therapeutic testing.

Functional polycystin-1 dosage governs autosomal dominant polycystic kidney disease severity

Katharina Hopp,[1] Christopher J. Ward,[2] Cynthia J. Hommerding,[2] Samih H. Nasr,[3] Han-Fang Tuan,[1] Vladimir G. Gainullin,[1] Sandro Rossetti,[2] Vicente E. Torres,[2] and Peter C. Harris[1,2]

[1]Department of Biochemistry and Molecular Biology, [2]Division of Nephrology and Hypertension, and [3]Division of Anatomic Pathology, Mayo Clinic, Rochester, Minnesota, USA.

Autosomal dominant polycystic kidney disease (ADPKD) is caused by mutations to *PKD1* or *PKD2*, triggering progressive cystogenesis and typically leading to end-stage renal disease in midlife. The phenotypic spectrum, however, ranges from in utero onset to adequate renal function at old age. Recent patient data suggest that the disease is dosage dependent, where incompletely penetrant alleles influence disease severity. Here, we have developed a knockin mouse model matching a likely disease variant, *PKD1* p.R3277C (RC), and have proved that its functionally hypomorphic nature modifies the ADPKD phenotype. While *Pkd1*$^{+/null}$ mice are normal, *Pkd1*$^{RC/null}$ mice have rapidly progressive disease, and *Pkd1*$^{RC/RC}$ animals develop gradual cystogenesis. These models effectively mimic the pathophysiological features of in utero–onset and typical ADPKD, respectively, correlating the level of functional *Pkd1* product with disease severity, highlighting the dosage dependence of cystogenesis. Additionally, molecular analyses identified p.R3277C as a temperature-sensitive folding/trafficking mutant, and length defects in collecting duct primary cilia, the organelle central to PKD pathogenesis, were clearly detected for the first time to our knowledge in PKD1. Altogether, this study highlights the role that in trans variants at the disease locus can play in phenotypic modification of dominant diseases and provides a truly orthologous PKD1 model, optimal for therapeutic testing.

Introduction

Autosomal dominant polycystic kidney disease (ADPKD [MIM no. 173900 for PKD1 and 613095 for PKD2]) is one of the most common monogenic disorders, with a prevalence of 1:400 to 1:1,000 (1, 2). It is genetically heterogeneous and has been linked to 2 loci, *PKD1* (16p13.3) and *PKD2* (4q21), mutated in approximately 85% and 15% of cases, respectively (3–5). Typically, the disease manifests with progressive bilateral cystic kidney enlargement, leading to end-stage renal disease (ESRD) in midlife; while, symptomatic polycystic liver disease, hypertension, and an enhanced level of intracranial aneurysms are other disease complications (6, 7).

The pathogenesis underlying the polycystic kidney disease (PKD) phenotypes is still unclear; however, various cellular defects have been suggested. For example, cyst development has been strongly associated with defects to the primary cilia, as evident from model systems and syndromic PKD forms, categorizing PKD as a ciliopathy (8, 9). Structural and functional cilia defects, including length abnormalities, have been characterized in several types of PKD, including the infantile onset autosomal recessive form (ARPKD, MIM no. 263200) (8–12). However, no clear ciliary structural abnormalities have been described in PKD1 (13–15). The majority of ciliogenes appear to maintain the structural integrity of the cilia or regulate protein trafficking to and from the organelle, while the PKD1 and PKD2 proteins, polycystin-1 (PC-1) and polycystin-2 (PC-2), respectively, are thought to form a complex on the primary cilium and act as a receptor (14, 16–19). One possibility is that the PC complex acts as a mechanosensor, signaling via a Ca^{2+} influx through PC-2, a TRP channel, after fluid flow detection by PC-1 (14, 16, 20). Additionally, urinary exosome-like vesicles (ELVs), which contain high levels of the polycystins, have been suggested to play a role in the mediation of signaling events at the primary cilia (11, 21, 22). However, the localization and function of PC-1 and PC-2 are still controversial, and various alternative cilia-related roles have been proposed (16, 23–26).

In addition to primary cilia defects, PKD cells exhibit many other cellular aberrations proposed to be associated with cystogenesis and/or cyst progression. These defects include, but are not limited to, dedifferentiation, increased proliferation and apoptosis, polarity defects, and altered gene expression that may be linked to increased intracellular cAMP, possibly associated with decreased intracellular Ca^{2+} (16, 27). The tubule segment that becomes cystogenic is also a point of debate in ADPKD. Traditionally, all tubule segments have been thought to be involved in disease, but the available data are limited and somewhat contradictory (28–30). Recently, treatments focused on lowering cAMP by targeting the arginine V2 vasopressin receptor (AVPR2), which is mainly expressed in the thick ascending limb of Henle and the collecting duct (CD), highlight the importance of clarifying this issue for the development of successful therapeutic interventions (28, 31, 32). Unfortunately, the currently available PKD1 rodent models are not ideal for the analysis of ADPKD pathogenesis, including determining the affected nephron segment or therapeutic testing. *Pkd1*-null animals die embryonically, and heterozygotes develop only very mild disease in old age, while conditional models do not reflect the disease development in human ADPKD due to the loss of all functional protein at one time (33–39). In addition, previously described hypomorphic mouse models develop very rapidly progressive disease, which is inadequate for therapeutic testing and does not reflect the gradual kidney enlargement typical of ADPKD (40, 41).

Conflict of interest: The authors have declared that no conflict of interest exists.
Citation for this article: *J Clin Invest.* 2012;122(11):4257–4273. doi:10.1172/JCI64313.

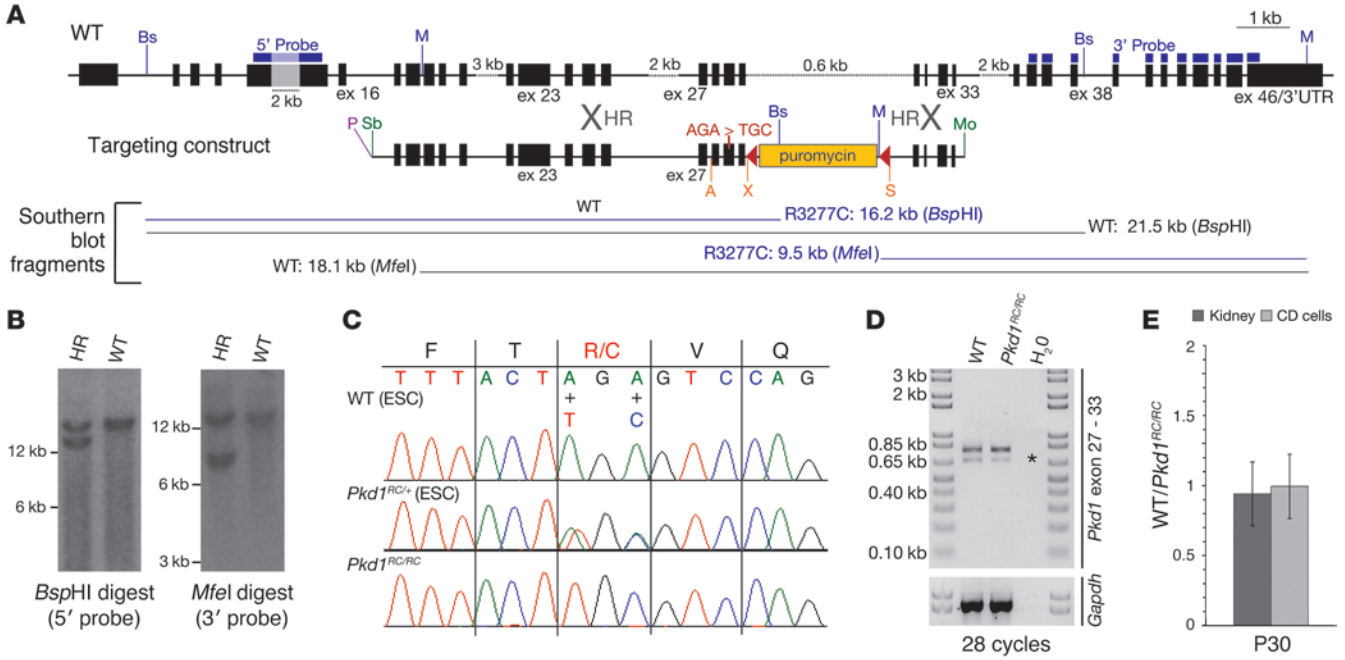

Figure 1

Generation of the *Pkd1* p.R3277C knockin mouse. (**A**) Diagram of the targeting construct used for injection into ESCs. Restriction sites flanking the construct are in green (Sb, *Sbf*I; Mo, *Mbo*I). The *Pkd1* p.R3277C mutation was introduced using the exact codon found in ADPKD probands (29, 59) (red). Restrictions sites used for introducing the mutation and the loxP-flanked (red triangles) selection cassette (yellow box) are in orange (A, *Adh*I; X, *Xho*I; S, *Sal*I). The restriction site used to linearize the targeting construct is shown in purple (P, *Pac*I). Restriction sites and probes used for Southern blotting are in blue (Bs, *Bsp*HI; M, *Mfe*I). (**B**) Representative Southern blot of successful HR in ESCs. (**C**) Sequencing chromatogram of WT and heterozygous ESC clones and a homozygous animal. (**D**) RT-PCR analysis across the mutation and the loxP-containing intron of a WT and a homozygous animal (after Cre-lox recombination). A normally seen alternative splice product, skipping exon 31 (in-frame change), was not significantly different between WT and homozygous animals (asterisk) (105) (PCR product, 762 bp; splice variant, 669 bp). (**E**) Quantification of PC-1 protein levels in whole kidney and CD cell lysate. PC-1 protein levels between WT and $Pkd1^{RC/RC}$ animals were not significantly different (WB not shown, see Figure 9 for more detail). Data are shown as a normalized ratio (loading control, γ-tubulin [TUBG1]) between WT and $Pkd1^{RC/RC}$ animals (n = 3/group). Statistical values were obtained by Student's t test; error bars indicate ± SD.

The severity of disease in ADPKD has been directly associated with the gene mutated; PKD1 on average leads to ESRD at approximately 54 years, while PKD2 leads to ESRD at approximately 74 years (42). The complete phenotypic spectrum, however, ranges from rare in utero–onset cases to patients with adequate renal function in old age; extreme heterogeneity that cannot be solely explained by genic effects (6, 43, 44). Some rare cases with early-onset ADPKD also develop tuberous sclerosis due to a contiguous deletion of *PKD1* and *TSC2* (MIM no. 600273), highlighting *TSC2* as a likely modifier of the PKD1 phenotype (45–47). Causes of extreme intrafamilial phenotypic variation include mosaicism or bilineal inheritance of a pathogenic *PKD1* and *PKD2* variant, but these do not account for the majority of cases with extreme ADPKD phenotypes (45, 48, 49).

The mechanism by which a heterozygous mutation results in cyst development is controversial (50). Complete loss of the ADPKD proteins in mice results in embryonic lethality and renal cyst development by E14.5 (33, 35, 51). Likewise, the corresponding human genotype is thought to be incompatible with life (52). One proposed mechanism, consistent with cyst development in null animals and the focal nature of cystogenesis, is a cellular recessive one, where each cyst is a clonal development resulting from complete polycystin loss. Somatic mutations to the WT *PKD1* or *PKD2* allele in individual cyst linings support this 2-hit mechanism, while the frequency and timing of this inactivation may explain some of the observed variable expressivity (53–56). Consistent with this, a *Pkd2* allele prone to somatic recombination results in progressive cystic disease, and PKD severity in conditional ADPKD mice differs radically depending on the age at complete polycystin inactivation (36–38, 57).

Although the cellular recessive mechanism is attractive, recent data indicate that the dosage level of the polycystins may be important. Homozygous *Pkd1* and *Pkd2* hypomorphs, with 13% to 33% correctly spliced *Pkd1* or *Pkd2*, are viable but develop progressive cystic disease in the kidney, liver, and pancreas, despite the presence of some functional polycystin (40, 41, 58). Additionally, recently described atypical ADPKD families highlight the role of putative incompletely penetrant *PKD1* or *PKD2* alleles. If inherited alone, these alleles are associated with mild PKD, while homozygotes or compound heterozygotes are viable and present with typical to severe disease, and in trans inheritance with a null allele causes in utero–onset disease (29, 59–62). However, proving the importance of specific alleles and analyzing the molecular mechanism is not possible from the study of a number of small families.

Here, we have taken an experimental approach by developing a knockin mouse model of a clinically proposed incompletely penetrant *PKD1* allele, p.R3277C (RC), to rigorously test a dose-de-

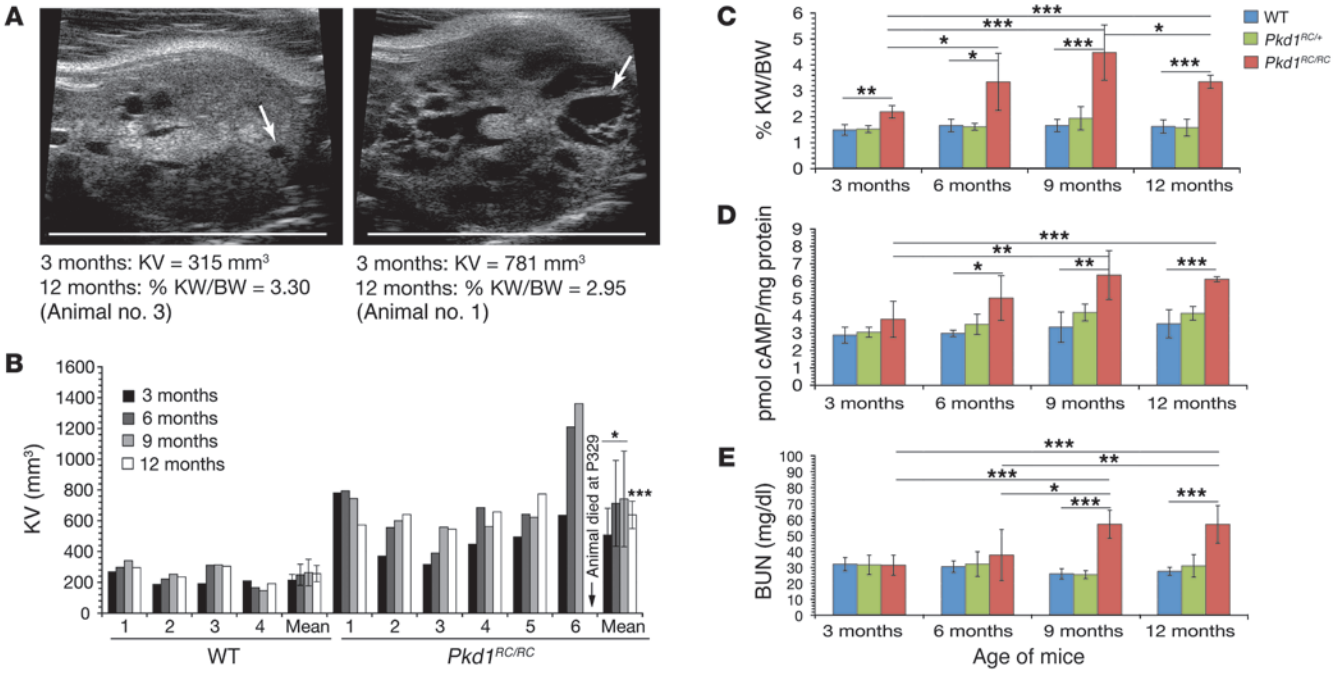

Figure 2

Homozygosity of the *Pkd1* p.R3277C allele results in progressive PKD with physiological characteristics comparable to those of human ADPKD. (**A**) Representative US M-mode images of $Pkd1^{RC/RC}$ mice. Kidneys with the mildest (left) and most severe disease (right) are shown at 3 months. Kidney cysts are visible as echolucent spots (arrows). Scale bars: 10 mm (left); 12 mm (right). (**B**) Quantification of US at 3, 6, 9, and 12 months of each individual animal and the mean of all animals. Significant differences between WT and homozygotes were seen at all time points. KV increased in most animals progressively, but variability among mice was observed. (**C**–**E**) Graphic representations of %KW/BW, cAMP, and BUN measured at 3, 6, 9, and 12 months (Supplemental Table 1). (**C**) %KW/BW increased progressively with cyst burden until 9 months, after which a significant decrease was observed, likely correlated with increased fibrosis (Table 1). (**D**) Similar to that in patients with ADPKD, cAMP levels rose with disease burden (16). (**E**) Increased kidney damage due to cystogenesis/fibrosis resulted in a significantly elevated BUN after 9 months. The data in **C**–**E** were obtained from the same group of animals at each time point (WT, $n = 4$; $Pkd1^{RC/RC}$, $n = 6$). Statistical values were obtained by the Student's *t* test (*$P < 0.05$, **$P < 0.01$, ***$P < 0.001$); error bars indicate ± SD.

pendent pathomechanism of cystogenesis and to investigate the role of these alleles in severe ADPKD. Furthermore, by generating models mimicking the pathophysiological features of typical and in utero–onset ADPKD, we have been able to study the process of cystogenesis in detail at the histological and molecular level, providing insights into pathogenesis and reagents to improve therapeutic options for this disorder.

Results

Generation of a knockin mouse model mimicking a clinical PKD1 allele. The *PKD1* p.R3277C allele was first identified in a consanguineous family of French ancestry in the United States, in which patients homozygous for the allele were viable but presented with mild to typical cystic disease (59). In 2 additional families with extreme intrafamilial disease variability, this allele segregated in trans with either a truncating or missense mutation, both resulting in very early-onset ADPKD (29, 59). These associated phenotypes suggested that the p.R3277C allele was incompletely penetrant. To date, 7 pedigrees (2 homozygous) have been identified with this variant, giving an ADPKD population allele frequency of 0.25% (ADPKD database [PKDB]; http://pkdb.mayo.edu). To rigorously test the role of such alleles in the variable expressivity of PKD1, we generated a knockin mouse model mimicking the exact codon usage seen in patients (*Pkd1* c.9805.9807AGA>TGC). The targeting construct was cloned from a 129Sv/E phage library using recombineering (Figure 1A and ref. 63). Embryonic stem cell (ESC) clones were screened for homologous recombination (HR) by Southern blotting, and the mutation was verified by Sanger sequencing (Figure 1, B and C). To exclude effects of the loxP-flanked puromycin selection cassette, all male germline transmitting chimeras were crossed with an oocyte-expressing Cre female (129S1/Sv-$Hprt^{tm1(cre)Mnn}$/J) to excise the selection cassette at the zygote stage. Subsequent RT-PCR analysis of the kidneys from homozygous animals ($Pkd1^{RC/RC}$ animals) showed no alteration in mRNA splicing or expression levels (Figure 1D). Likewise, PC-1 expression was unaltered between WT and $Pkd1^{RC/RC}$ animals when analyzing kidney whole cell lysates or kidney-derived CD cells (in kidney, PC-1 expression in $Pkd1^{RC/RC}$ was 94% ± 2.30% of WT, $P = 0.450$; in CD cells, PC-1 expression in $Pkd1^{RC/RC}$ was 99% ± 2.30% of WT, $P = 0.605$; Figure 1E). This suggested that the defect in the action of this allele was likely at the level of functional protein.

Mice homozygous for the Pkd1 p.R3277C allele develop mild but progressive PKD. We first set out to characterize the *Pkd1* p.R3277C allele in homozygosity (Figures 2 and 3, Supplemental Figure 1, and Supplemental Table 1; supplemental material available online with this article; doi:10.1172/JCI64313DS1), mimicking the published consanguineous family with adult-onset ADPKD (59). From a heterozygous cross, we observed the expected Mendelian ratios of offspring (data not shown), implying that *Pkd1*

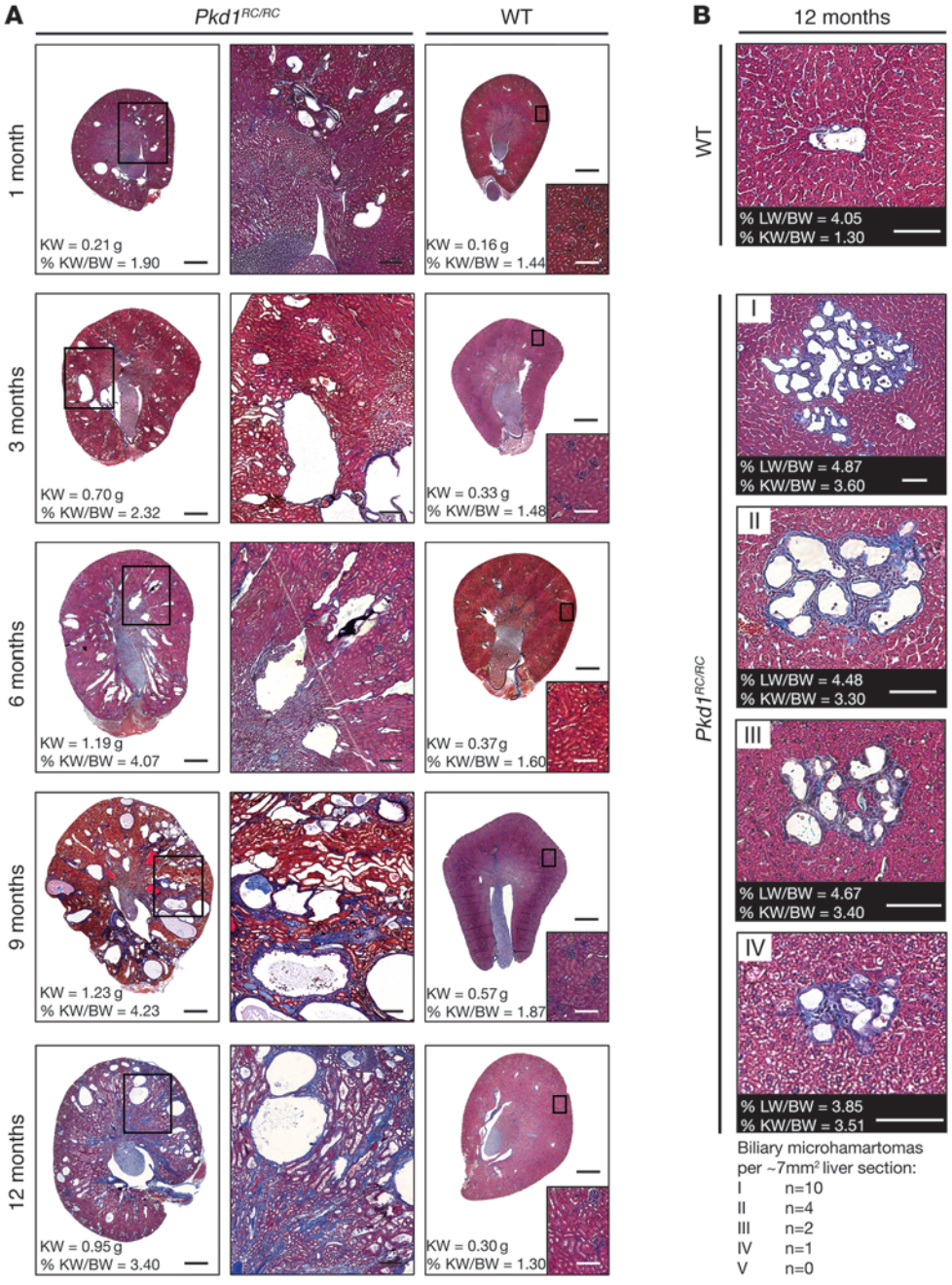

Figure 3
Histology of homozygous *Pkd1* p.R3277C animals mimics typical ADPKD. (**A**) Representative Masson Trichrome histology sections of *Pkd1*$^{RC/RC}$ and WT kidneys at 1 to 12 months show that cysts developed progressively with age. At later time points, an increased level of fibrosis was noted (12 months; Table 1). Scale bars: 1 mm (kidney cross-section, WT, and *Pkd1*$^{RC/RC}$); 250 μm (*Pkd1*$^{RC/RC}$ magnified region [images in second column]); 200 μm (WT magnified region [insets]). (**B**) Masson Trichrome histology sections of 12-month-old *Pkd1*$^{RC/RC}$ and WT livers (no significant difference between percentage of liver weight [LW] per body weight [%LW/BW] of WT animals and homozygotes was noted). Four out of five homozygous animals showed ductal plate malformations, including microhamartomas of varying severity. These cystic lesions are progenitors of the liver cysts often found in patients with ADPKD (69). Scale bars: 100 μm.

p.R3277C is not a fully penetrant allele. To analyze disease presentation and progression, we initially followed 4 WT and 6 *Pkd1*$^{RC/RC}$ littermates by ultrasonography (US). At 3 months of age, cysts ranging from 0.3 to 2.5 mm in diameter were visible in all *Pkd1*$^{RC/RC}$ animals (Figure 2A). Kidney volumes (KVs) were estimated from 3D M-mode renderings, and it was determined that *Pkd1*$^{RC/RC}$ KVs increased progressively over time in most animals and were significantly increased compared with those of WT littermates at all investigated time points (Figure 2B and Supplemental Table 1); although, there was noticeable variability between these outbred animals (Figure 2B; e.g., animal no. 3 vs. no. 6). The increase in KV was directly correlated with the progressive but variable increase in cyst burden seen histologically at 3, 6, 9, and 12 months (Figure 3A and Supplemental Figure 1) and reflected in a steady increase in percentage of kidney weight per body weight (%KW/BW) (Figure 2C and Supplemental Table 1). At 12 months of age, we noted a slight decrease in KV and %KW/BW, which was likely associated with increased fibrosis (3.3% of kidney area at 3 months vs. 20.3% at 12 months; Table 1), highlighted by increased Masson Trichrome staining (Figure 3A and Supplemental Figure 1). A similar decrease in %KW/BW associated with increased fibrosis has been observed at earlier ages in other hypomorphic *Pkd1* models and in late stages of human ADPKD (40, 41, 64). This steady increase in fibrosis seems mainly to correlate with cyst growth, although some fibrosis is evident when there is minimal cystogenesis. A number of factors, including epithelial paracrine release of

Table 1
Summary of kidney composition by area, using lectin and fibrosis markers[A]

Pkd1$^{RC/del2}$	Individual animals			Mean (%)	SD	*P* value
	1	2	3			
P1	**% Stained area/kidney area**					–
LTA-PT cysts	20.7	32.8	34.1	29.2	7.4	–
DBA-CD cysts	1.9	4.2	6.4	4.2	2.2	–
Unstained cysts	0.1	0.5	0.3	0.3	0.2	–
Noncystic kidney tissue	77.3	62.5	59.3	66.4	9.6	–
%KW/BW	2.51	2.67	3.21	–	–	–
P12	**% Stained area/kidney area**					**P1 vs. P12**
LTA-PT cysts	11.1	9.6	7.5	9.4	1.8	0.0108
DBA-CD cysts	23.9	31.0	35.6	30.2	5.9	0.00203
Unstained cysts	2.2	3.2	2.5	2.6	0.5	0.00189
Fibrotic tissue	2.3	3.2	5.1	3.5	1.5	–
Noncystic kidney tissue	60.5	53.0	49.3	54.3	5.7	0.135
%KW/BW	5.94	5.86	7.91	–	–	–
P25	**% Stained area/kidney area**					**P12 vs. P25**
LTA-PT cysts	2.5	3.1	3.1	2.9	0.3	0.00387
DBA-CD cysts	53.3	46.2	54.3	51.3	4.4	0.00771
Unstained cysts	14.0	18.9	15.2	16.0	2.6	8.94×10^{-4}
Fibrotic tissue	20.7	28.0	24.0	24.2	3.7	8.11×10^{-4}
Normal kidney tissue	9.5	3.8	3.4	5.5	3.4	2.23×10^{-4}
%KW/BW	24.26	31.20	27.69	–	–	–

Pkd1$^{RC/RC}$	Individual animals			Mean (%)	SD	*P* value
	1	2	3			
P1	**% Stained area/kidney area**					–
LTA-PT cysts	15.8	16.3	18.6	16.9	1.5	–
DBA-CD cysts	1.3	2.4	0.7	1.5	0.9	–
Unstained cysts	0.1	0.3	0.0	0.1	0.1	–
Noncystic kidney tissue	82.8	81.0	80.7	81.5	1.1	–
%KW/BW	1.90	2.67	2.08	–	–	–
P12	**% Stained area/kidney area**					**P1 vs. P12**
LTA-PT cysts	2.9	2.1	2.4	2.5	0.4	8.18×10^{-5}
DBA-CD cysts[B]	12.9	15.2	24.0	17.4	5.8	0.00941
Unstained cysts	1.2	1.8	2.0	1.7	0.4	0.00289
Noncystic kidney tissue	83.0	80.9	71.6	78.5	6.0	0.444
%KW/BW	2.48	2.90	3.91	–	–	–
3 months	**% Stained area/kidney area**					**P12 vs. 3 months**
LTA-PT cysts	0.3	0.5	0.9	0.6	0.3	0.00258
DBA-CD cysts[B]	2.9	5.4	4.9	4.4	1.3	0.0197
Unstained	1.1	4.0	2.8	2.6	1.4	0.325
Fibrotic tissue	3.7	1.9	4.3	3.3	1.2	–
Normal kidney tissue	92.0	88.3	87.0	89.1	2.6	0.0488
%KW/BW	2.27	2.32	2.18	–	–	–
12 months	**% Stained area/kidney area**					**3 months vs. 12 months**
LTA-PT cysts	5.8	1.6	11.4	6.3	4.9	0.115
DBA-CD cysts	11.5	16.7	12.5	13.6	2.8	0.00659
Unstained cysts	5.0	14.3	6.4	8.5	5.0	0.122
Fibrotic tissue	19.4	9.7	31.9	20.3	11.1	0.0578
Normal kidney tissue	58.4	57.7	37.8	51.3	11.7	0.00542
%KW/BW	3.30	3.60	3.40	–	–	–

[A]Quantification was performed on a cross section from 1 kidney per animal. Consecutive cross sections were stained for each marker. The percentage of area of cysts originating from the distal tubule (PNA) or the loop of Henle (THP) was consistently below 1% and was not included in the calculations.
[B]The percentage of cyst area per kidney area was decreased due to a rapid increase in overall kidney weight between P12 and 3 months.

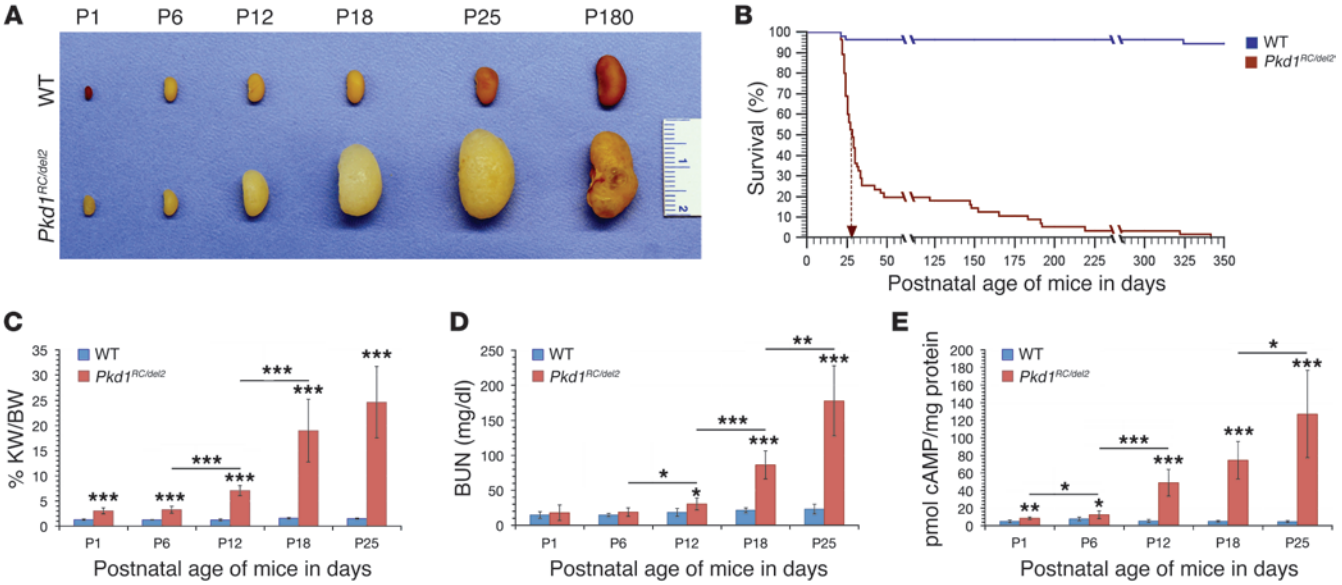

Figure 4

Pkd1$^{RC/null}$ mice develop in utero/early-onset ADPKD. (**A**) Gross images of WT and *Pkd1*$^{RC/del2}$ kidneys from P1 to P180, illustrating early-onset/rapidly progressive disease. After P25, the kidney size decreased, likely due to increased fibrosis (Figure 5 and Table 1). The ruler depicts centimeters. (**B**) Kaplan-Meier curve of WT and *Pkd1*$^{RC/del2}$ mice. Eighty percent of *Pkd1*$^{RC/del2}$ mice died before P50 (median survival, P28 [arrow]; n = 55/group). (**C**–**E**) Graphical representations of %KW/BW, BUN, and cAMP from P1 to P25 of *Pkd1*$^{RC/del2}$ animals (Supplemental Table 2). (**C**) %KW/BW was significantly increased as early as P1 (3%) and rapidly climbed to 25% by P25. (**D**) BUN levels rose beyond the physiological average as early as P18. (**E**) cAMP levels were significantly above normal by P1. Values in **C**–**E** were obtained from $n \geq 5$ at each time point for both WT and *Pkd1*$^{RC/del2}$ mice. P180 data can be found in Supplemental Table 2. Statistical values were obtained by the Student's t test (*$P < 0.05$, **$P < 0.01$, ***$P < 0.001$); error bars indicate ± SD.

proinflammatory and profibrotic mediators, epithelial production of extracellular matrix proteins, and epithelial-mesenchymal transition, likely promote the fibrosis (65).

Analysis of the onset of cystogenesis showed that the *Pkd1*$^{RC/RC}$ animals had histologically visible cysts as early as E16.5 (Supplemental Figure 2). This compares with approximately E14.5 in *Pkd1*$^{null/null}$ mice and highlights that, although these animals are viable, the time of cyst initiation is not radically different from that in the null state (35, 51). Renal cystic enlargement was accompanied by an increase in renal cAMP, significant after 6 months, as described in other rodent models and patients with ADPKD (Figure 2D and refs. 16, 39, 66, 67). Additionally, increasing kidney damage, presumably due to both the development and expansion of cysts and fibrosis (Table 1), caused a measurable decline in kidney function, detected by a rise in blood urea nitrogen (BUN) above the physiological range (18.6–32.9 mg/dl) by 9 months (Figure 2E and refs. 66–68). Further, histological analysis showed that at 12 months most *Pkd1*$^{RC/RC}$ animals developed multiple ductal plate malformations, seen as microhamartomas (Figure 3B). These cystic lesions have been reported previously in *Pkd1*$^{+/null}$ animals, are characteristic of human ADPKD, and are the progenitors of the liver cysts found in the majority of patients (34, 69). *Pkd1*$^{RC/+}$ animals did not develop any renal cysts, have any significant differences in renal function from WT, or develop any liver phenotype by 1 year of age (data not shown).

This analysis of homozygous animals showed that the *Pkd1* p.R3277C allele is pathogenic, as all analyzed animals developed PKD, dismissing the notion that it may be one of the many silent, nonsynonymous variants detected in *PKD1* (PKDB, http://pkdb.mayo.edu). On the other hand, the viability of the homozygotes showed that the allele is not fully penetrant, proving for the first time to our knowledge the existence of incompletely penetrant *PKD1* alleles and highlighting their role as a disease modifier.

The Pkd1 p.R3277C allele modifies the Pkd1$^{+/null}$ *phenotype to early-onset disease.* To directly test the proposed modifier role of *Pkd1* p.R3277C and to mimic the genotype associated with human in utero–onset disease, we crossed *Pkd1*$^{RC/+}$ animals with a well-established *Pkd1*-null model, *Pkd1*$^{+/del2}$ (Figures 4 and 5, Supplemental Figure 3, Supplemental Table 2, and refs. 51, 59). Again, we observed the expected Mendelian ratios of offspring (data not shown), but in this case the progression of disease was much more aggressive. *Pkd1*$^{RC/del2}$ animals showed enlarged kidneys by P1, visible from gross anatomy, and a significantly greater %KW/BW compared with that of WT littermates (3.05% vs. 1.29%; Figure 4, A and C, and Supplemental Table 2). The %KW/BW increased rapidly from approximately 3% at P1 to approximately 25% at P25. In comparison, the %KW/BW at P1 of *Pkd1*$^{RC/del2}$ animals was significantly higher than that of homozygous animals at 3 months (P = 0.01). At the histological level, cysts were visible as early as E15.5, and both the number and size of cysts increased in an exponential fashion to at least P25 (Figure 5, Figure 6B, Table 1, and Supplemental Figures 2 and 3). Interestingly, multiple glomerular cysts were detectable at the early time points, highlighting a clear similarity with human in utero–onset ADPKD (Figure 5, insets, and refs. 59, 70). The rapidly expansive PKD was also associated with premature death, first noted at P20, and with a median survival at P28; 80% of animals were dead by P50 (Figure 4B). The cause of death was

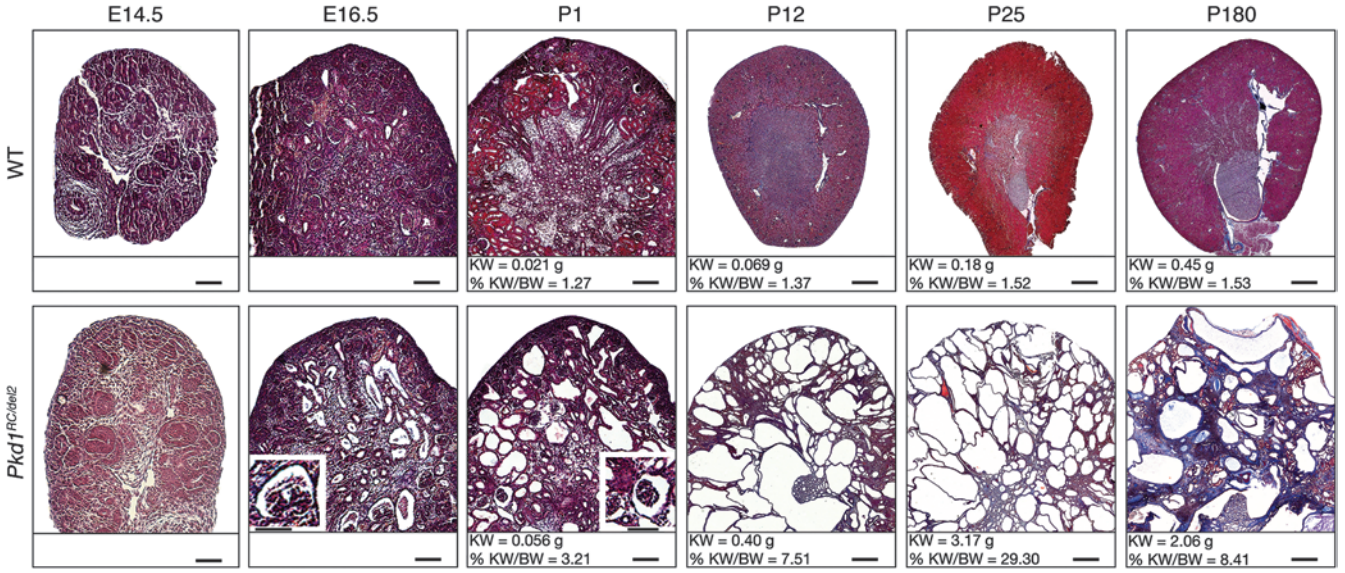

Figure 5
Histology of *Pkd1*$^{RC/del2}$ mice highlights early-onset and rapidly progressive cystic disease. Representative Masson Trichrome sections of *Pkd1*$^{RC/del2}$ and WT kidneys from E14.5 to P180. Kidney cysts were clearly visible as early as E16.5 (a few cysts were present at E15.5; Supplemental Figure 2) and rapidly increased in number/size with age (Table 1). Glomerular cysts were present as early as E16.5 (insets) (59). The kidneys of animals with longer survival (P180) were highly fibrotic, with little obvious healthy tissue. Scale bars: 100 μm (E14.5 to P1); 500 μm (P12); 750 μm (P25 and P180); 50 μm (insets).

likely associated with renal failure, as indicated by marked renal cystic enlargement (70.2% of kidney area by P25; Table 1), increased fibrotic index (24.2% by P25; Figure 5 and Table 1), and uremia evident by a significant increase in BUN at P12 (Figure 4D and Supplemental Table 2). Animals surviving beyond P25 exhibited further evidence of disease progression with significantly elevated BUN levels (~178 mg/dl [P25] vs. ~314 mg/dl [P180], $P = 0.006$; Supplemental Table 2) and a decline in %KW/BW, which is likely associated with an increase in fibrotic tissue (~25% [P25] vs. ~9% [P180]; Figure 4A, Figure 5, and Supplemental Table 2), as with the *Pkd1*$^{RC/RC}$ mice at 12 months. The reason that approximately 20% of animals survived much longer is unclear, but it is of note that this outbred population had milder disease during the explosive cyst expansion period (P12–P25), suggesting a less critical role for PC-1 during adulthood. Consistent with a dosage-dependent disease mechanism, *Pkd1*$^{RC/del2}$ animals had a much more rapid rise in cAMP, with P1 mice having higher cAMP levels than 12-month-old *Pkd1*$^{RC/RC}$ mice ($P = 0.0042$) and BUN levels above the physiological average as early as P18 (Figure 2; Figure 4, D and E; Supplemental Tables 1 and 2; and ref. 68). In addition, *Pkd1*$^{RC/del2}$ animals presented with osteopenia and left ventricular hypertrophy (LVH), known extrarenal phenotypes observed in other *Pkd1* models and patients with ADPKD (Supplemental Figure 4 and refs. 71–73). A decrease in trabecular and cortical bone mass was observed in *Pkd1*$^{RC/del2}$ males and females at P25, likely correlating with reduced PC-1 function in osteoblasts, but possibly also associated with secondary hyperparathyroidism (Supplemental Figure 4A, data on females not shown, and refs. 71, 72). Heart weight was also significantly increased, with the myocardium of the left ventricle significantly thickened (Supplemental Figure 4B) and evidence of LVH, possibly due to hypertension in the P25 *Pkd1*$^{RC/del2}$ animals with advanced cystic disease. No intracranial aneurysms were noted.

This compound heterozygous model clearly demonstrates the role of *Pkd1* p.R3277C as a modifying allele. The *Pkd1*$^{+/del2}$ mice did not exhibit an ADPKD phenotype, lacking renal cysts and functional changes in kidneys at 1 year of age (data not shown), contrasting dramatically with the rapid disease progression in *Pkd1*$^{RC/del2}$ animals (51). These data prove that in trans inheritance of a null and this incompletely penetrant allele, without the requirement of other genetic events, results in early-onset ADPKD, suggesting a clear dosage pathomechanism of cyst initiation and/or progression.

Pkd1 p.R3277C mice show a switch in tubular cyst origin correspondent with age and an increase in proliferation. The models described here developed cysts due to a consistent reduction of PC-1, compared with conditional knockouts, in which only the segments engineered to be null for PC-1 became cystic. Consequently, answering the question of where and when cysts develop in our model is relevant to human PKD1. Using immunofluorescence (IF) markers for each tubule segment (lotus tetragonolobus agglutinin [LTA] – proximal tubule [PT], peanut agglutinin [PNA] – distal tubule, Tamm-Horsfall glycoprotein [THP] – loop of Henle, and Dolichos biflorus agglutinin [DBA] – CD), we examined the cystic origin throughout disease development. In *Pkd1*$^{RC/del2}$ animals at P1, 82% of cysts were of PT and 17% of cysts were of CD origin. However, by P25, these animals had only 6% PT and 76% CD cysts. Interestingly, by this time point, 18% of cysts (16% of kidney area) could not be recognized by any of the tubule markers used, including PNA and THP (Figure 6, A and B, and Table 1), suggesting that they had become dedifferentiated. The switch in cyst origin was also noticeable when looking at cyst area rather than cyst number, with the area occupied by PT cysts falling from 29.2% at P1 to 2.9% at P25. During the same period, CD cysts rose from 4.2% of kidney area to 51.3% (Table 1). In *Pkd1*$^{RC/RC}$ mice, a similar switch was observed; at P1, 90% of cysts were of PT and 8%

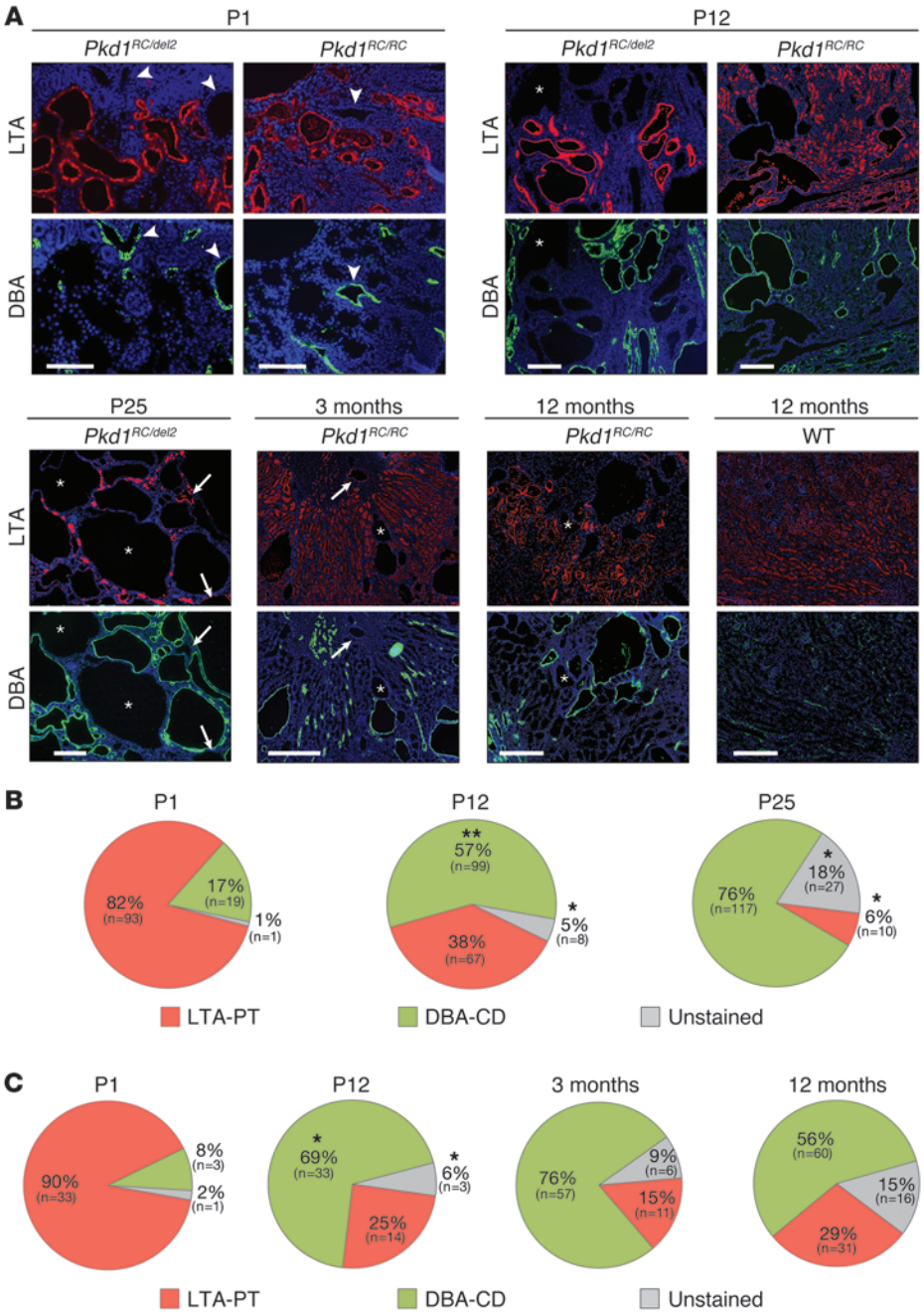

Figure 6

Pkd1 p.R3277C mice show a switch in tubular cyst origin corresponding to age. (**A**) IF lectin labeling of PT (LTA) and CD (DBA). During early kidney development (P1), cysts originated mainly from PT in $Pkd1^{RC/del2}$ and $Pkd1^{RC/RC}$ animals, with only rare CD cysts (arrowheads). Later in development (P12), a switch to more CD cysts occurred that became more prominent after kidney development (P25, $Pkd1^{RC/del2}$; 3 months, $Pkd1^{RC/RC}$), with only a few remaining PT cysts (arrows). With disease progression, an increasing number of cysts seemed to dedifferentiate. Asterisks indicate a lack of labeling with tubule markers. Scale bars: 100 μm (P1); 200 μm (P12); 300 μm (P25); 500 μm (3 months and 12 months). (**B**) Quantification of cyst origin at P1, P12, and P25 for $Pkd1^{RC/del2}$ animals and (**C**) P1, P12, 3 months, and 12 months for $Pkd1^{RC/RC}$ animals (n = 3; Table 1). Significance is based on cyst number. Statistical values were obtained by the Student's t test ($^*P < 0.05$, $^{**}P < 0.01$). Data are not shown for distal tubule (PNA) and loop of Henle (THP), as they accounted for <1% of the total cyst number.

were of CD origin, while at 3 months, 76% were of CD and 15% were of PT origin (Figure 6, A and C, and Table 1). Interestingly, at 12 months of age, the percentage of PT cysts increased as compared with that at 3 months, from 15% to 29%; however, most of the PT cysts corresponded to mildly dilated tubules, whereas the majority of larger cysts were either of CD origin (56%, 13.6% of area) or dedifferentiated (15%, 8.5% of area; Figure 6, A and C, and Table 1). The PT dilatation at this stage may reflect acquired renal cystic disease associated with advanced renal insufficiency as seen in human ADPKD (74, 75).

This analysis of both models shows a consistent shift in cyst origin, with a predominance of PT kidney cysts during kidney development, which continues in the mouse until approximately 2 weeks postnatally, to a predominance of CD cysts once the kidney has fully developed (37). This is consistent with PT cysts predominating in early-onset ADPKD cases, with a similar shift from PT to CD cysts associated with completion of kidney development in ARPKD (28, 29, 39, 76, 77). The observation that the majority of adult cysts are of CD origin correlates with the AVPR2 antagonists showing some benefit in ADPKD (31, 32, 78).

PCNA staining of CD tubules and cysts in P18 $Pkd1^{RC/del2}$ animals highlighted that cyst expansion/size correlates with an increase in proliferation (Figure 7 and Supplemental Table 3). Proliferation was greatest in the largest cysts (5.50% vs. 3.09% in small cysts, P = 0.002), but, notably, even nondilated tubules showed increased proliferation compared with WT (1.71% vs.

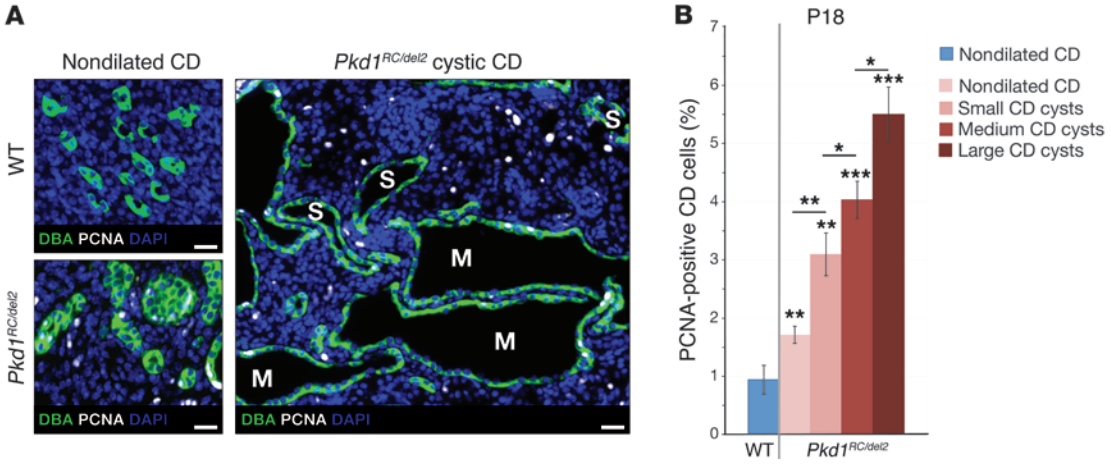

Figure 7
Cystogenesis of *Pkd1*$^{RC/del2}$ mice is associated with an increase in proliferation. (**A**) Representative images of kidney tissue from P18 *Pkd1*$^{RC/del2}$ mice, indicating increased proliferation in noncystic and cystic CDs (DBA) compared with that in WT. Reports on associations between cyst expansion and proliferation are controversial, but analysis of the CD showed a clear increase in cell division (36, 37, 79). Scale bars: 20 μm. (**B**) Graph summarizing data of 100 nondilated CD cysts and 20 small (<50 cells [S]), 10 medium (50–200 cells [M]), and 5 large (>200 cells) CD cysts (Supplemental Table 3) (n = 3/group). Statistical values were obtained by the Student's t test (*P < 0.05, **P < 0.01, ***P < 0.001); error bars indicate ± SD.

0.94%, P = 0.009). The role of proliferation to cyst expansion in ADPKD is a controversial one, but when analysis is limited to tubular/cystic epithelia, increased cell division clearly occurs (36, 37, 79).

The Pkd1 p.R3277C allele is associated with elongated CD primary cilia. In syndromic forms of PKD, the mutated proteins are proposed to regulate ciliary protein trafficking and, hence, influence ciliogenesis; therefore, structural ciliary abnormalities, including length defects, have been associated with these diseases (8–10). However, in PKD1, the majority of studies have not detected cilia length defects, but the data are not conclusive, as these studies were largely conducted by light microscopy using cultured cells (14, 15, 80, 81). To analyze whether PC-1 may have a role in ciliary maintenance, we analyzed renal CD and bile duct cilia length using scanning electron microscopy (SEM). Cilia of nondilated and cystic CDs were significantly longer in P25 *Pkd1*$^{RC/del2}$ animals (mean = 4.98 μm) and 12-month-old *Pkd1*$^{RC/RC}$ animals (mean = 3.02 μm) compared with those in WT controls (mean = 1.98 μm; Figure 8A and Supplemental Table 4 [WT vs. *Pkd1*$^{RC/del2}$, P = 0.0012; WT vs. *Pkd1*$^{RC/RC}$, $P = 5.65 \times 10^{-4}$]), with a significant difference between *Pkd1*$^{RC/del2}$ mice and their homozygous counterparts (P = 0.0066). Interestingly, these length defects were not related to cystic dilatation, since measurements in cystic and noncystic CDs in both animal models did not significantly differ (Supplemental Table 4). Furthermore, this observation was independent of age, since the length of WT cilia did not change from P25 to 12 months of age (Supplemental Table 4). Cilia within normal bile ducts did not vary significantly between genotypes (Figure 8B, Supplemental Table 5, and ref. 79). However, bile duct cilia were elongated in 1 microhamartoma that was found by SEM ($P = 1.49 \times 10^{-6}$; Figure 8B and Supplemental Table 5). Therefore, within the kidney, the dosage dependence of cilia length abnormality indicates that the level of functional PC-1 is directly associated with the observed ciliary defect, whereas in the liver, cilia elongations seem related to bile duct abnormalities.

The Pkd1 p.R3277C allele alters PC-1 cleavage and folding/maturation. PC-1 is a multidomain glycoprotein that is cleaved at a G protein–coupled receptor proteolytic site (GPS; Figure 9A and refs. 82, 83). After cleavage, the N-terminal product (NTP) and the C-terminal product (CTP) are thought to remain tethered and functionally act together (Figure 9A and ref. 83). It has also been reported that endogenous PC-1 is observed as 2 distinct glycoforms, endoglycosidase H–resistant (EndoH-resistant) (NTP**) and -sensitive (NTP*) forms (84). This implies a difference in protein trafficking of these glycoforms, as EndoH resistance is obtained in the trans-Golgi, in which high-mannose oligosaccharides are converted to complex saccharides by the addition of N-acetylglucosamine to form secreted or membrane-bound, mature, forms of the protein (85). We confirmed these findings by Western blot (WB) analysis of kidney membrane protein with 2 products found in the untreated sample, one being the EndoH stable form (no shift in size [NTP**]), and the other being the sensitive form that reduces in size upon EndoH treatment (loss of all N-linked glycosylation [NTP*]; Figure 9B). Treatment with peptide-N-Glycosidase F (PNGaseF), an enzyme that removes all N-linked sugars independent of maturation status, reduced the size of the 2 products to that of the EndoH-sensitive form, showing that the difference in size of the 2 untreated products is only due to variable glycosylation status. Analysis of urinary ELVs, showed that it is the EndoH-resistant PC-1 that is present in these vesicles (Figure 9B and refs. 21, 22). Comparison of ELV PC-1 with an exogenously expressed PC-1 GPS cleavage mutant (E2771K; Figure 9A) showed that the PNGaseF-treated full-length PC-1 was much larger than the treated ELV product, indicating that only the cleaved product is found in ELVs (NTP**; Figure 9C). Also, only the cleaved product (NTP) was observed in kidney tissue preparations, consistent with the significance of this cleavage event for normal function (83).

To analyze the possible pathomechanism of *Pkd1* p.R3277C, we first investigated whether the allele altered PC-1 cleavage by using an exogenously expressed C-terminally tagged PC-1 construct

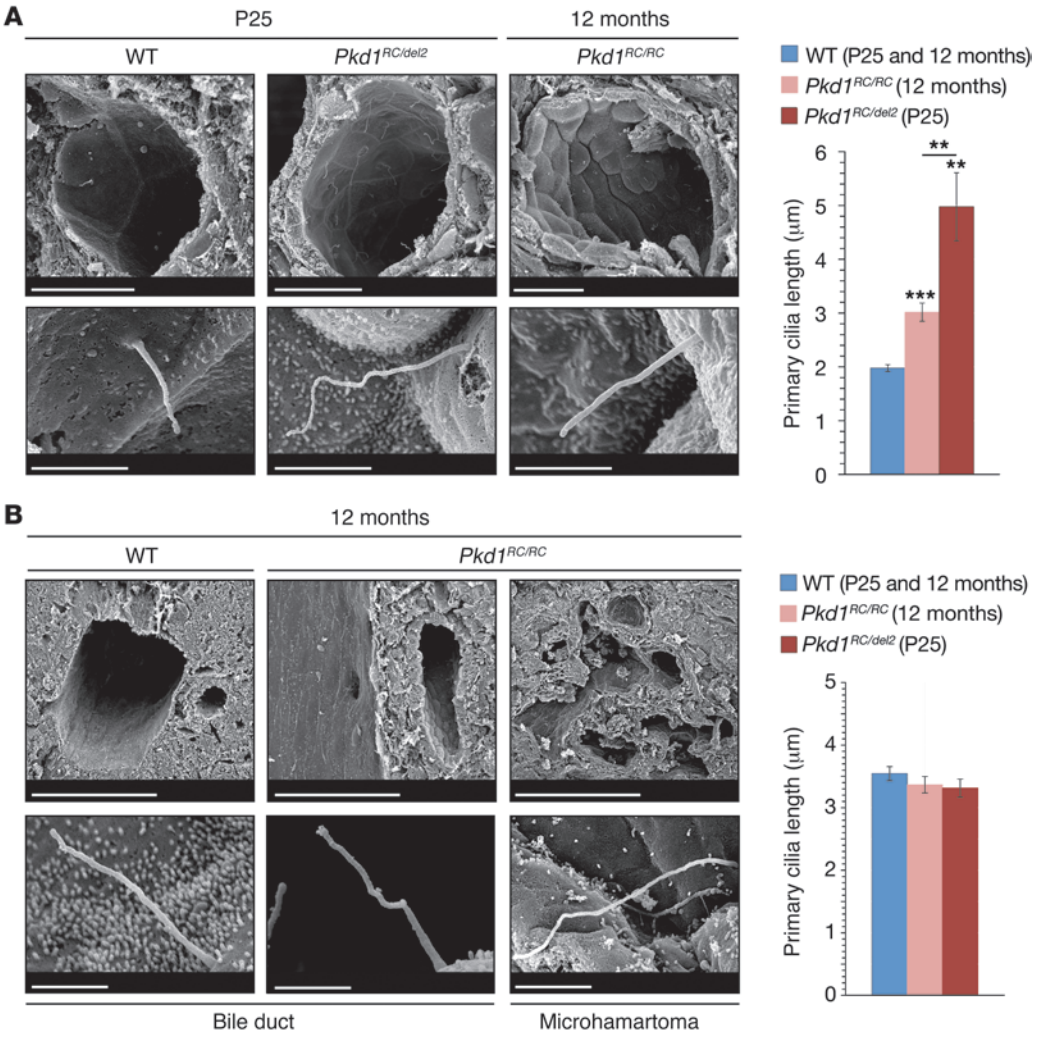

Figure 8

Primary cilia are elongated in *Pkd1* p.R3277C CDs but not normal bile ducts. SEM analysis of primary cilia length (**A**) in the CDs (Supplemental Table 4) and (**B**) bile ducts (Supplemental Table 5) of WT, $Pkd1^{RC/del2}$, and $Pkd1^{RC/RC}$ mice at the ages indicated ($n = 3$ animals/group). (**A**) Representative SEM images of CDs and individual cilia. Scale bars: 2 μm (bottom row); 10 μm (WT, top row); 15 μm ($Pkd1^{RC/del2}$ and $Pkd1^{RC/RC}$, top row) (left). Graph summarizing >100 cilia measurements (~40 cilia in nondilated, ~30 in dilated, and ~30 in cystic CDs) in mutant animals and >50 cilia of nondilated CDs in WT animals (P25 and 12 months). The level of functional *Pkd1* inversely correlated with cilia length, indicating a role of PC-1 in cilia maintenance (right). (**B**) Representative SEM image of WT and $Pkd1^{RC/RC}$ bile duct and one microhamartoma. Bile duct cilia of the microhamartoma were significantly elongated (6.24 ± 1.57 μm, $P < 0.001$) (left). Scale bars: 1 μm (WT and $Pkd1^{RC/RC}$, bottom row); 2 μm (microhamartoma, bottom row); 50 μm ($Pkd1^{RC/RC}$, top row); 100 μm (WT and microhamartoma, top row). Graph summarizing >50 cilia measurements of >5 bile ducts per animal (right). Statistical values were obtained by the Student's *t* test (**$P < 0.01$, ***$P < 0.001$); error bars indicate ± SD.

(Figure 9A). WB using an antibody to the C-terminal V5 epitope tag highlighted significantly reduced levels of cleaved p.R3277C PC-1 compared with WT (~76% of WT, Figure 9D). However, we also tested a second suspected incompletely penetrant *Pkd1* allele (p.R2220W) that was found in trans with *PKD1* p.R3277C resulting in early-onset ADPKD, and this PC-1 product was far more resistant to cleavage (~26% of WT) (29). The p.R2220W variant is localized within the receptor for egg jelly domain (REJ), a domain previously shown to be important for GPS cleavage (83). These results suggested that inefficient cleavage may be a pathomechanism associated with some incompletely penetrant PC-1 alleles but may not be central to the reduced function of *Pkd1* p.R3277C; hence, we investigated further possible mechanisms. Since *PKD1* p.R3277C is 2 amino acids from the second transmembrane domain (TMII; Figure 9A), we tested whether TMII integrates appropriately into the lipid bilayer in the presence of this missense change. Using exogenous expression of a partial PC-1 construct with a C-terminal glycosylation reporter, we assayed successful TMII integration. However, no noticeable difference in membrane integration ability was found compared with WT (Supplemental Figure 5).

Since the cleaved, mature PC-1 is found in urinary ELVs, it was possible to use urinary ELVs from WT and mutant mice to assay possible folding or trafficking defects. We isolated ELVs from a 12-hour urine collection of 1- and 12-month-old $Pkd1^{RC/RC}$ mice and found from WB analysis that they had an approxi-

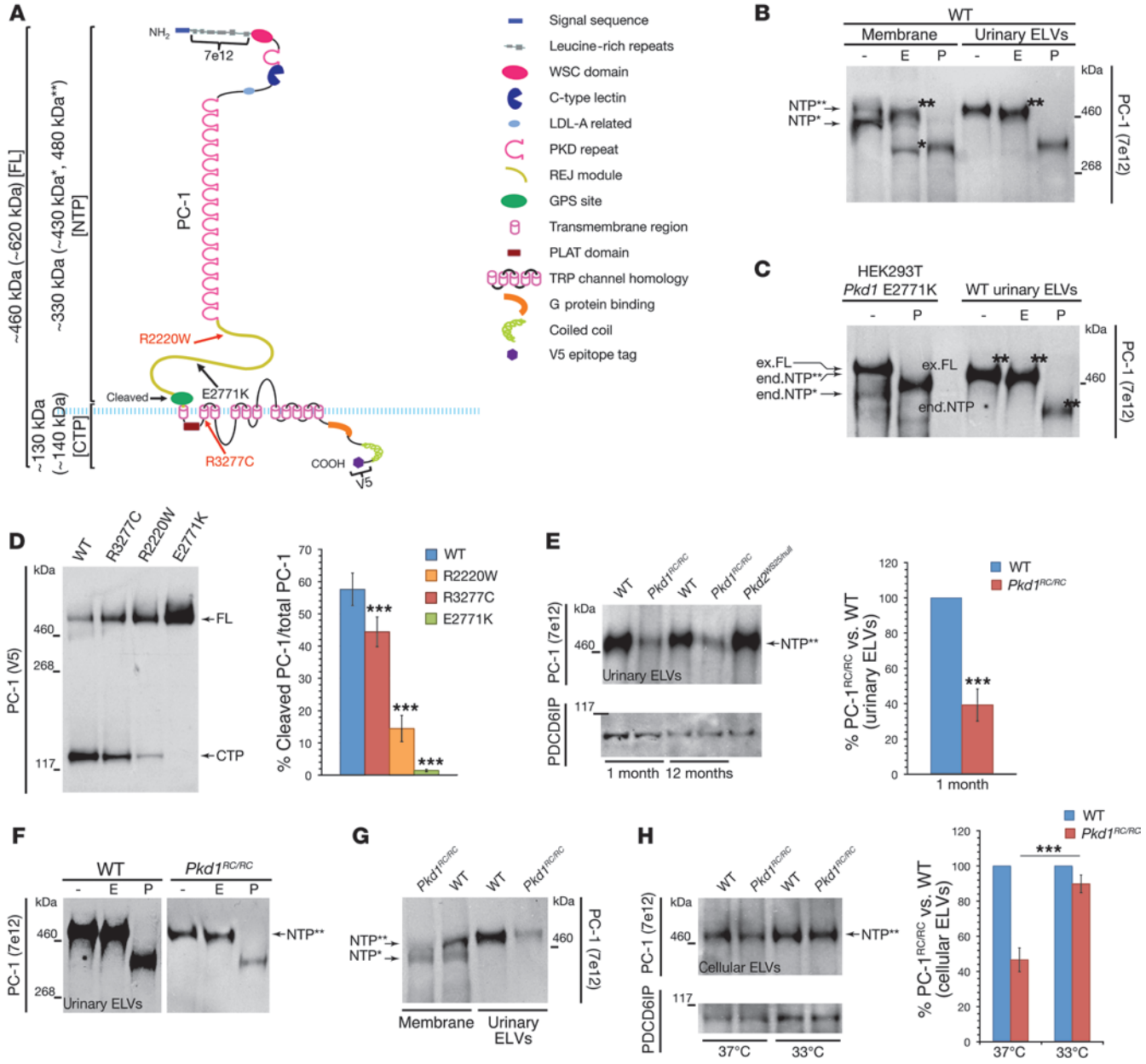

Figure 9

Pkd1 p.R3277C is a temperature-sensitive folding/maturation mutant. (**A**) The PC-1 protein (full-length [FL]) is cleaved into NTPs and CTPs (estimated sizes of glycosylated PC-1 are indicated in parentheses) (82–84). The positions of the incompletely penetrant variants (p.R3277C, p.R2220W) and the cleavage mutant p.E2771K are shown (29, 59, 83). NTP*, EndoH-sensitive, immature; NTP**, EndoH-resistant, mature. (**B**) WB of PC-1 showing the 2 glycoforms in kidney membranes and only the mature form in urinary ELVs. (**C**) WB of the exogenously expressed cleavage mutant *Pkd1* p.E2771K (ex) and WT urinary ELVs (83). The endogenous (end) PC-1 protein is also seen at a low level. The endogenous, mature, cleaved PC-1 (NTP**) runs at a size similar to the ex.FL PC-1 p.E2771K (immature form). (**D**) WB and cleavage quantification ($n = 6$ transfections) of exogenously expressed WT and mutant forms of PC-1 shown in **A**. (**E**) WB and quantification of PC-1 levels in WT and $Pkd1^{RC/RC}$ urinary ELVs at 1 and 12 months ($n = 4$ urine collections of 6 animals/group). ELVs from $Pkd2^{WS25/null}$ mice show PC-1 levels in *Pkd2* cystic kidneys (57). (**F**) EndoH assay of urinary $Pkd1^{RC/RC}$ ELVs (analyzed on separate gels as indicated by the white line). (**G**) WB of $Pkd1^{RC/RC}$ kidney membrane preparation and urinary ELVs compared with WT. (**H**) WB and quantification ($n = 3$ experiments) of PC-1 in cell media–isolated ELVs from primary CD cells isolated from WT and $Pkd1^{RC/RC}$ P30 kidneys at 37°C and 33°C. PDCD6IP is an ELV expressed control protein (21). E, EndoH; P, PNGaseF. Statistical values were obtained by the Student's *t* test (***$P < 0.001$); error bars indicate ± SD.

mately 61% reduction of the mature, EndoH-resistant PC-1 glycoform compared with WT; all mutant PC-1 found in ELVs was EndoH stable, highlighting that the mutant protein trafficked appropriately (Figure 9, E and F). Analysis of ELVs collected from $Pkd2^{WS25/-}$ mice that have a similar level of cystogenesis as the analyzed $Pkd1^{RC/RC}$ mice showed unaltered levels of PC-1 NTP** compared with WT mice, highlighting that the reduction in PC-1 in the $Pkd1^{RC/RC}$ mice is not due to the presence of cystic disease (57).

To confirm these findings in the kidney, we performed WB of kidney membrane preparations of 1-month-old littermates. Consistent with the results from the urinary ELVs, *Pkd1*$^{RC/RC}$ animal kidneys showed a reduced level of the EndoH stable PC-1 NTP** compared with WT (Figure 9G).

These results suggested that the reduction of EndoH stable PC-1 p.R3277C may result from a maturation defect between the ER and the trans-Golgi or from a folding defect within the ER (85). To investigate a possible folding defect, primary cells isolated from *Pkd1*$^{RC/RC}$ kidney CDs were grown at a reduced temperature to create an environment more permissive for protein folding (33°C, compared with 37°C) (86). Indeed, the temperature shift increased the relative amount of the EndoH stable PC-1 glycoform in cellular ELVs to a level close to that in WT ELVs and significantly different from that at the higher temperature (Figure 9H, $P = 0.00089$ [*Pkd1*$^{RC/RC}$, 33°C vs. 37°C], $P = 0.00017$ [37°C, WT vs. *Pkd1*$^{RC/RC}$], $P = 0.025$ [33°C, WT vs. *Pkd1*$^{RC/RC}$]). Consequently, we propose that the *Pkd1* p.R3277C allele is a temperature-sensitive folding mutant. However, accumulation of the mutant protein was not sufficient to trigger ER stress (Supplemental Figure 6). Therefore, due to the folding defect (and reduced cleavage), p.R3277C results in an approximately 60% reduction of mature PC-1 in *Pkd1*$^{RC/RC}$ mice.

Discussion

In this study, we set out to understand the etiology and pathomechanism associated with the phenotypic heterogeneity of PKD1, which at its extremes ranges from mild PKD in old age without renal insufficiency to in utero lethality (6, 43, 44). Emerging family data suggested that in trans inheritance of a null and an incompletely penetrant *PKD1* allele could result in the devastating early-onset phenotype (29, 59–61). To rigorously test this theory, we developed and characterized a knockin mouse model mimicking a naturally occurring *PKD1* variant, p.R3277C, highlighted by recent family studies (29, 59). Mirroring the human studies, *Pkd1*$^{RC/RC}$ animals developed gradual cystic disease over 1 year, while *Pkd1*$^{RC/null}$ mice had rapidly progressive disease, proving the significance of this combination of alleles. This simple pathomechanism is consistent with the description by Zerres (43), nearly 20 years ago, of a high recurrence risk of severe disease in siblings of an early-onset case in families with otherwise typical ADPKD. Data from a handful of additional families, highlighting other possible incompletely penetrant alleles, indicate a broader applicability, but studies of larger populations and better definition of these alleles are needed to determine the full importance of in trans inheritance to explaining early-onset disease (29, 59–62). Indeed, other mechanisms, such as modifier loci beyond the disease gene and environmental factors, also significantly influence disease variability. Early-onset severe ADPKD has been linked to contiguous deletion of *PKD1* and *TSC2* as well as co-inheritance of a *PKD1* and a *HNF1B* or *PKHD1* allele, highlighting the fact that digenic inheritance may account for some of the phenotypic variability seen in ADPKD (45–47, 62). Further, 3 SNPs in *DKK3* have been associated with severity of renal disease in a candidate gene association study, while nongenetic factors, such as male hormones, caffeine, and smoking, have been suggested as risk factors in ADPKD (87–89). Careful analysis is now required to determine the significance of each of these elements with respect to disease severity and to identify other genetic and environmental disease modifiers.

Insights from our model systems into the etiology of in utero ADPKD and the functional analysis of the mutant PC-1 provide further clues to the underlying pathomechanism of typical ADPKD. Although cystogenesis is often considered a cellular recessive process, in our case both the *Pkd1*$^{RC/RC}$ and *Pkd1*$^{RC/del2}$ animals have a *Pkd1* mutation to both alleles, making it unlikely that a somatic *Pkd1* mutation is required for cyst initiation. Instead, it seems more plausible that the dosage of PC-1 is underlying disease severity, and, by expression analysis of PC-1 in ELVs (an abundant site of polycystin expression that is readily isolated), we have precisely quantified the levels of mature protein associated with progressive adult disease (~40% in *Pkd1*$^{RC/RC}$) and inferred a level of mature protein associated with rapidly progressive, early-onset disease (approximately 20% in *Pkd1*$^{RC/del2}$ and ref. 21). Hence, it seems reasonable to propose that ADPKD severity is directly related to PC-1 dosage; adult-onset disease is usually caused by a 50% PC-1 reduction (haploinsufficiency), while further reductions due to variants on the "normal" allele cause severe early-onset presentations. The progressive PKD associated with transgenic miRNA reduction of *Pkd1* by 60% to 70% is consistent with the dosage model presented here (90). Although, there is strong evidence of a second-hit mechanism, with detected somatic mutations in large cysts, we propose that they are not necessary for cyst initiation and instead may play a role in cyst progression by providing cysts a growth or survival advantage (53–56).

The combination of a dosage pathomechanism in ADPKD and the realization that variants of the disease gene inherited from the "normal" parent can significantly influence the PKD1 phenotype have profound implications for understanding the variable expressivity of ADPKD. We have focused on extreme early-onset disease through co-inheritance of an incompletely penetrant and fully penetrant allele, but some alleles may have a lesser effect on the level of functional PC-1 and result in less extreme effects, such as ESRD in early adulthood. While efforts to identify genetic modifiers of the PKD1 phenotype through genome-wide association studies and exome or whole-genome sequencing are underway, it seems plausible that variants to the "normal" *PKD1* allele are a major disease modifier and that complex allelic inheritance is relevant more generally to the variable expressivity of ADPKD. Hence, better classification of variants with incompletely penetrant potential will be of increasing prognostic value. Further, it seems likely that this pathomechanism is important to the phenotypic variability of other haploinsufficient, dominant diseases, although the large array of "normal" variants cataloged at *PKD1* indicate that it may be an extreme example (PKDB, http://pkdb.mayo.edu) (91, 92).

Our models not only allow the genetic mechanism of disease to be analyzed but also provide insight into the pathophysiology. We have shown that increased proliferation is an important factor in cyst expansion. Of further interest, in both models cyst initiation occurred embryonically (E15.5–E16.5), but PKD developed much more quickly in the model with the lower level of PC-1. It is not known whether this dosage difference influences the rate of cyst initiation or expansion, but in this study, it seems that dosage may be relevant in both instances. Previous comparisons of PKD1 and PKD2 concluded that it was the rate of cyst initiation rather than rate of expansion that makes PKD1 more severe (88). Interestingly, analysis of conditional *Pkd1* models showed that PKD severity altered radically depending upon the time of gene inactivation, with a tipping point between rapid and

slow expansion of disease roughly corresponding to the completion of kidney development (37). Hence, developing tubules with high proliferative indices may be more sensitive to PC-1 reduction/loss. The rate of epithelial cell proliferation during development may also explain the switch with completion of kidney development from predominately PT to CD cysts observed in our study and previously reported in human ADPKD (28–30). The proliferation of immature early tubules (S-shaped bodies) is very high and remains high throughout embryonic life (93). In later development, when the epithelium differentiates into nephron segments recognizable by light microscopy, the proliferative index decreases substantially but remains elevated in the distal nephron and CD, whereas it becomes very low in the PT (93). In pediatric and adult kidneys, proliferative indices are very low in all tubular segments but remain higher in the CD compared with those in PT (94). Thus, the underlying rate of epithelial cell proliferation may explain both the increased susceptibility of the developing kidney to cystogenesis and the switch from predominantly PT to predominantly CD cysts. Understanding this switch is important, since theoretical considerations have highlighted that embryonic cysts, by growing at faster rates compared with cysts initiated later in life, contribute majorly to the total cyst burden (95).

A major argument for the 2-hit hypothesis is that the cyst development in ADPKD is focal, each the result of an individual somatic mutation (50). However, in the models presented here in which somatic mutations to the normal allele are not likely to be important, cyst development is still focal. This implies that a threshold model is important where stochastic factors, such as variation in the PC-1 expression level from cell to cell and so-called third hits (perhaps to be considered second hits now), such as renal damage or other factors triggering proliferation, may be key to driving a cell or segment of tubule into cystic transformation (96–98).

The role primary cilia play in ADPKD cystogenesis remains controversial, with the majority of studies focused on downstream signaling defects (16). Little attention has been given to the structural appearance of ADPKD primary cilia, despite length and other structural defects detected in other PKD-related ciliopathies (8–15). Here, we report for the first time to our knowledge a clear PC-1 dosage-dependent increase in cilia length in normal and cystic CDs. Increased cilia length has been associated with enhanced cAMP levels and injury/inflammation, the latter of which may be associated with the observed increase in cilia length within the microhamartoma; however, within the kidney, it is of interest that we observed the length increase independent of the cystogenic state of the tubule (80, 99, 100). This highlights a potential direct role of PC-1 in cilia maintenance. Alternatively, the length increase could be a compensatory response to reduced functional PC-1, extending the platform hosting the flow or ELV detector when less PC-1 is present. Furthermore, the clear description of the processing of PC-1 into mature and immature EndoH forms presented here should stimulate further study of the localization of this large and complex protein. Here, we have shown that just the resistant form can be found in urinary ELVs; however, the glycoform found on primary cilia or the plasma membrane remains unknown (21).

One of the most valuable features of this study is likely the development of new *Pkd1* models, which are well suited for therapeutic testing in comparison with current models. As described in the Introduction, the present fully inactivating models are unsatisfactory, and since conditional models lose all functional PC-1 at one time, with the affected kidney segment dictated by the Cre promoter, they do not reflect human disease development. Previously described hypomorphic models have approximately 70% to 80% PC-1 reduction, leading to very rapid disease with high levels of fibrosis early in life, similar to our approximately 80%-reduction model ($Pkd1^{RC/del2}$), and thus leaving a short therapeutic window (40, 41). Our 60%-reduction model ($Pkd1^{RC/RC}$) appears to best mimic human ADPKD (over a shorter timescale) with a 9-month progressive expansion and then a slight reduction in KV associated with fibrosis as ESRD approaches (101). Other similarities include those observed physiologically, with increased cAMP and elevation of BUN indicating renal insufficiency after 9 months, and histologically, with progressive cyst development and expansion, and a switch from PT to CD cysts following renal development. The temperature-sensitive nature of p.R3277C suggests that interventions to promote more efficient folding of PC-1 may increase the level of functional protein. This indicates that, in addition to the current experimental therapies that focus on cAMP and other signaling defects, chaperone-enhancing or proteasome-inhibiting strategies may also be effective in a subset of patients with missense mutations to *PKD1* or *PKD2* (102, 103). Last, a dosage model of ADPKD suggests that approaches to increase the level of the normal *PKD1* (*PKD2*) allele in patients with typical ADPKD, even by a modest amount, could have a dramatic clinical benefit.

Methods

Generation of the knockin construct. The targeting template for the *Pkd1* p.R3277C (murine *Pkd1* p.R3269C) knockin construct was obtained from a 129/Sv genomic phage library, using a cDNA probe spanning exons 19–23. The identified phage (11.1 kb, *Pkd1* IVS16-IVS34) was cloned into pZErO^{-2TM}. oligo.PGK-TK (pZErO^{-2TM} plus oligo [*Pac*I, *Sbf*I, *Mfe*I] plus thymidine kinase gene). A β-lactamase expression cassette flanked with a 3′ *Sal*I site was recombineered into IVS30, using the DY380 *E. coli* strain (63). The intronic position of the cassette was assessed (ASD Intron Analysis and ESEfinder 3.0) to minimize the possibility of disrupting spliceosome binding sites or the branch point. The mutation and the loxP-flanked puromycin cassette were introduced using a pZErO^{-2TM} shuttle vector system (*Ahd*I, *Xho*I, *Sal*I polylinker). An amplified 129/Sv *Pkd1* fragment, spanning from the *Ahd*I site (IVS27) to the end of the β-lactamase cassette (*Xho*I; IVS30), was cloned into the shuttle vector, and *Pkd1* p.R3277C was introduced using the Phusion Site-Directed Mutagenesis Kit (NEB) (29, 59). The loxP-flanked puromycin cassette, including Southern blotting restrictions sites, was excised from pBS.DAT-LoxStop and cloned into the shuttle vector using *Xho*I/*Sal*I sites. The modified genomic sequence, including the loxP-flanked selection cassette, was excised from the shuttle vector (*Ahd*I/*Sal*I) and exchanged with the original sequence within the targeting construct (pZErO^{-2TM}.PGK-TK) to generate the complete construct. The construct was linearized with *Pac*I (Figure 1A).

Generation and genotyping of knockin mice. The targeting construct was electroporated into 129/Sv ESCs by the Mayo Gene Targeting Core as previously described (104). Successful HR was confirmed by Southern blotting using a 5′ (2.9 kb; exon 15) and 3′ probe (2.0 kb; exons 36–46; Figure 1A) and 1.5 μg of ESC DNA digested with either *Bsp*HI (5′ probe) or *Mfe*I (3′ probe) (Figure 1A). ESC clones positive for HR were verified by sequencing and injected into blastocysts of pseudopregnant C57BL/6 females. Germline transmission was obtained with 2 clones. All experiments were performed on generation F_3 animals (C57BL/6) from 1 clone (generation F_2 was first crossed against the Cre-recombinase expressing line, 129S1/Sv-$Hprt^{tm1(cre)Mnn}$/J, to remove the selection cassette). $Pkd1^{+/del2}$ was a fully congenic C57BL/6 line (51).

Genotyping of all *Pkd1* p.R3277C animals was performed by *Hinf*I digest of a 719-bp PCR fragment spanning IVS27–exon 30. The p.R3277C mutation destroys the *Hinf*I site (WT, 439 bp, 280 bp; *Pkd1* p.R3277C, 719 bp). $Pkd1^{+/del2}$ mice were provided by Shigeo Horie (Department of Urology, Teikyo University Hospital, Kanto/Tokyo, Japan) and genotyped using two separate PCR reactions, mutant (474 bp) and WT (380 bp).

RT-PCR analysis. RT-PCR analysis (n = 3) was performed on RNA isolated from 1-month-old, flash-frozen WT and $Pkd1^{RC/RC}$ kidneys (Figure 1C), from left tibias of P25 WT and $Pkd1^{RC/del2}$ males (Supplemental Figure 4A, tibias were sonicated in 200 μl TRIzol before RNA isolation), or from cultured CD cells isolated from 1-month-old WT and $Pkd1^{RC/RC}$ kidneys (Supplemental Figure 6). RNA was isolated using the Qiagen RNeasy Kit, and RT was performed with the SuperScript III RT Kit (Invitrogen).

For *Pkd1* cDNA analysis, exons 27–33 were amplified (762 bp or 669 bp, splice variant skipping exon 31; ref. 105). RT analysis of osteocalcin, *Runx2*, and *Gapdh* was performed as previously described (71). RT analysis of ER stressors was performed using primers to the murine mRNA (*Hspa5*, 335 bp; *Herpud1*, 301 bp; *Xbp1*, 205 bp; *Actb*: 397 bp). Fragments were quantified using ImageJ software.

Histological analysis. Animals were sacrificed by carbon dioxide exposure (Mayo IACUC guidelines) prior to organ harvest, and body/organ weights were recorded. Histology of 4% paraformaldehyde–fixed tissue was processed and H&E/Masson trichrome stained by the Mayo Department of Pathology. All tissues were examined by an experienced pathologist (S.H. Nasr). Kidneys (right), livers, pancreata, hearts, lungs, spleens, testes, and brains were analyzed from P25 and P180 $Pkd1^{RC/del2}$ animals and 12-month-old $Pkd1^{RC/RC}$ animals. At all other time points, only kidneys were reviewed. At each time point, a minimum of 6 animals (3 per gender) were reviewed. Slides were observed using ×5 and ×10 objectives (Zeiss AxioObserver, Carl Zeiss). In cases in which the size of the histological section exceeded the visual field, single images were fused (AxioVision software).

US and KV measurements. US analysis of the right kidneys from WT (2 females, 2 males) and $Pkd1^{RC/RC}$ mice (3 females, 3 males) at 3, 6, 9, and 12 months was performed as described previously (106) with the following modifications: 40-MHz scan head, 3D step size of 0.05 mm, and focal depth of 0.09 mm. KV calculations were performed by reconstructing a 3D image of kidney traces at a step size of 0.5 mm (VisualSonics software). A mean of 2 KV measurements was recorded. No cysts were found in $Pkd1^{RC/+}$ animals at 12 months.

BUN/cAMP measurements. Blood plasma was separated (6,000 *g*, 15 minutes at 4°C) from blood isolated by cardiac puncture and used for the BUN assay (BUN-Urea, BioAssay Systems), and cAMP levels (Direct cAMP EIA Kit, ENZO) were measured from 100 to 200 mg of flash-frozen kidney (left). Both assays were performed following the manufacturer's protocol.

Micro-CT analysis. Micro-CT was performed on the right femurs of 3 P25 WT and $Pkd1^{RC/del2}$ males using the μCT35 system (Scanco Medical) at the Mayo Bone Histomorphometry Core. The femur was oriented along the rotational axis of the scanner in a 70-kVP/180-mAs x-ray tube and scanned at an integration time of 300 ms. Sections were taken at an element size of 0.007 mm (trabecular bone, 233 sections; cortical bone, 50 sections). Cortical percentage of bone volume/tissue volume (%BV/TV) was determined by tracing the bone outline of all 50 sections. The %BV/TV values are the mean of duplicate measurements.

IF labeling. Tissues were prepared for IF labeling as previously described (10). Biotinylated-LTA, -DBA, and -PNA (1:250, Vector Laboratories); TH (1:200, Santa Cruz Biotechnology Inc.); and PCNA (1:100, Santa Cruz Biotechnology Inc.) labeling was performed as indicated (11, 79), with secondary antibodies (Alexa Fluor, Invitrogen) used at a 1:500 dilution. Cyst number and area were estimated using ImageJ software. A dilated tubule was counted as a cyst, if its area exceeded 0.02% of the total kidney area (~500 μm^2, dependent on age). For cyst number, cysts were counted using the Analyze Particle/Cell Counter plug-in for ImageJ (Figure 6, B and C). For percentage of cyst area, the kidney area (medulla plus cortex) was measured, followed by measurement of the cyst area of individually stained or unstained cysts. Fibrotic area was measured using the Masson Trichrome section. All area calculations were preformed using the Analyze Particle (IF images) or the Measure and Label (Masson Trichrome) plug-in for ImageJ. Results were expressed as percentage of stained area per kidney area (Table 1). For PCNA analysis, the Axio Vision software was used (Figure 7). Single kidney cross sections from 3 nonlittermate mice were labeled and analyzed (consecutive sections from the same kidney were used for each marker).

SEM. SEM imaging was performed on the left kidney and the right liver lobe as described previously (11, 79). CDs were identified based on known morphological features, and bile ducts were identified based on their proximity to a portal vein/hepatic artery (107). For kidney SEM, approximately 50 cilia were imaged from each WT animal (two P25 animals and one 12-month-old animal), and cilia of cystic (~30; n > 6), dilated (~30; n > 6), and nondilated (~40; n > 10) CDs were imaged from each mutant animal (three P25 $Pkd1^{RC/del2}$ animals and three 12-month-old $Pkd1^{RC/RC}$ animals). For liver SEM, approximately 50 cilia from at least 5 different bile ducts per animal were imaged from each genotype. In both cases, kidney and liver, genotype-blinded cilia length measurements were made with ImageJ software.

ELV isolation and whole kidney membrane/cell lysate preparation. Urinary ELVs were isolated as described previously (104). Three male and three female WT or $Pkd1^{RC/RC}$ animals were placed in metabolic cages for 12 hours to collect 10 ml urine (overall experimental, n = 4). Isolation of urinary ELVs from the $Pkd2^{WS25/null}$ model as controls was possible because Stefan Somlo (Yale School of Medicine, New Haven, Connecticut, USA) provided us with the model. Cellular ELVs were similarly isolated from primary CD cells grown in 20 ml (six 15-cm plates = 120 ml total) serum-free media for 3 days. Whole kidney membrane preps from 1-month-old WT or $Pkd1^{RC/RC}$ animals were prepared as described previously (Figure 9, B and G, ref. 104). Whole kidney lysates were prepared from 1-month-old WT or $Pkd1^{RC/RC}$ flash-frozen kidneys (n = 3) after homogenization with mortar and pestle followed by 18G, 21G, and 25G needle homogenization. The homogenate as well as CD cells (n = 3/group; Figure 1D and Supplemental Figure 4B) were lysed using RIPA buffer (Millipore).

Cleavage and membrane integration assay. The cleavage assay (n = 6) was performed using a full-length *Pkd1* construct with a C-terminal V5 tag (Figure 9D). To introduce mutations, the fragment was shuttled into pZErO^{-2TM} (*Eco*RI/*Sac*II). The membrane integration assay (n = 3) was modified from a previously described protocol using a PC-1 transmembrane glycosylation construct provided by Robin Maser (Clinical Laboratory Sciences, University of Kansas Medical Center, Kansas City, Kansas, USA; Supplemental Figure 5 and ref. 108). In both experiments, the *Pkd1* variant was introduced using the Phusion Site-Directed Mutagenesis Kit (NEB), and the WT and mutant constructs were transfected into HEK293T cells following manufacturer protocol (Polyfect, Qiagen). Cells were lysed 24 hours after transfection using RIPA buffer (Millipore).

Primary cell culture/temperature shift assay. Primary CD cells were harvested from 1-month-old WT and $Pkd1^{RC/RC}$ kidneys (2 animals per harvest, nonlittermates) as described previously (104), with the following modifications: after sieving the cells through 80-μm mesh, the flow through was

transferred onto a 40-μm mesh to capture CD cells. Cells were plated on six 15-cm BD BioCoat type IV collagen-coated dishes (BD Biosciences). Cells were passaged after 3 days and placed either at 37°C or 33°C. At 70% confluence, the culture media were replaced with serum-free media and collected 3 days later for ELV preparation (n = 4).

Western blotting. Western blotting was performed on 3%–8% TA gels (Invitrogen) for 2.75 hours (cleavage/transmembrane assay, ELVs) or 4.5 hours (membrane preparations) at 150 V at 4°C; loading amounts are as follows: exogenously expressed protein (20 μg), ELVs (10 μg), membrane preparations (60 μg), Molecular Weight Marker, HiMark (Invitrogen). For ER stress analysis and PC-1 WT/p.R3277C quantification, WB was performed on 4%–12% Bis-Tris gels (Invitrogen) for 1 hour at 200 V at room temperature (ER stress, 20 μg; PC-1 quantification, 50 μg protein). Gels were transferred to 0.45-μm nitrocellulose membranes at 15 V overnight at 4°C. Quantified blots (PC-1 levels, cleavage/transmembrane assay, ELVs, ER stress) were developed using the LICOR system (Odyssey Sa) to assure linear quantification of the signal intensity; all other blots were probed with HRP-conjugated secondary antibodies (Southern Biotech). The following primary antibodies were used: 7e12 (1:500 dilution) (lab owned), PK (1:1,000) (Serotec), PDCD6IP (1:250) (ProteinTech), HSPA5 (1:5,000) (BD Biosciences), P4HB (1:1,000) (Cell Signaling), and TUBG1 (1:5,000) (γ-tubulin, Sigma-Aldrich). All EndoH and PNGase assays were performed according to the manufacturer's protocol (NEB).

Statistics. Statistical significance was determined using 2-tailed, unpaired, unequal sample size, equal variance Student's t test. $P < 0.05$ was considered significant.

Study approval. These animal studies were conducted under the "ADPKD: models of polycystic kidney disease protocol" (#A16709), which was reviewed and approved by the IACUC of the Mayo Clinic, in accordance with NIH, USDA, and AAALAC guidelines.

Acknowledgments

We thank the Mayo Gene Targeting Core, especially Jan van Deursen, Ming Li, and Wei Zhou, for help in generating the chimeric knockin mice; Jennifer Westendorf and Meghan McGee-Lawrence for assisting with the bone morphology analysis; Bruce Knudsen for training K. Hopp at US analysis of mouse kidneys; the Mayo Clinic Electron Microscopy Core, especially Scott Gamb and Jason Bakeberg, for training K. Hopp to use SEM on kidney tissue; Xiaofang Wang for her assistance with the cAMP assays; and Tatyana Masyuk for help with the PCNA staining. This work was supported by an AHA predoctoral fellowship to K. Hopp (11Pre5250020), NIDDK grant DK058816, the Mayo Translational PKD Center (DK090728), and the Zell Family Foundation.

Received for publication April 23, 2012, and accepted in revised form August 23, 2012.

Address correspondence to: Peter C. Harris, Division of Nephrology and Hypertension, Mayo Clinic, 200 First Street SW, Rochester, Minnesota 55905, USA. Phone: 507.266.0541; Fax: 507.266.9315; E-mail: harris.peter@mayo.edu.

1. Iglesias CG, Torres VE, Offord KP, Holley KE, Beard CM, Kurland LT. Epidemiology of adult polycystic kidney disease, Olmsted County, Minnesota: 1935–1980. *Am J Kidney Dis*. 1983;2(6):630–639.
2. Dalgaard OZ. Bilateral polycystic disease of the kidneys; a follow-up of two hundred and eighty-four patients and their families. *Acta Med Scand Suppl*. 1957;328:1–255.
3. Mochizuki T, et al. PKD2, a gene for polycystic kidney disease that encodes an integral membrane protein. *Science*. 1996;272(5266):1339–1342.
4. Rossetti S, et al. Comprehensive molecular diagnostics in autosomal dominant polycystic kidney disease. *J Am Soc Nephrol*. 2007;18(7):2143–2160.
5. [No authors listed]. The polycystic kidney disease 1 gene encodes a 14 kb transcript and lies within a duplicated region on chromosome 16. The European Polycystic Kidney Disease Consortium. *Cell*. 1994;77(6):881–894.
6. Harris PC, Torres VE. Polycystic kidney disease, autosomal dominant. In: Pagon RA, et al., eds. *GeneReviews*. Seattle, Washington, USA: University of Seattle; 1993(updated 2011):NBK1246.
7. Torres VE, Harris PC, Pirson Y. Autosomal dominant polycystic kidney disease. *Lancet*. 2007;369(9569):1287–1301.
8. Hildebrandt F, Benzing T, Katsanis N. Ciliopathies. *N Engl J Med*. 2011;364(16):1533–1543.
9. Gascue C, Katsanis N, Badano JL. Cystic diseases of the kidney: ciliary dysfunction and cystogenic mechanisms. *Pediatr Nephrol*. 2011;26(8):1181–1195.
10. Tammachote R, et al. Ciliary and centrosomal defects associated with mutation and depletion of the Meckel syndrome genes MKS1 and MKS3. *Hum Mol Genet*. 2009;18(17):3311–3323.
11. Woollard JR, et al. A mouse model of autosomal recessive polycystic kidney disease with biliary duct and proximal tubule dilatation. *Kidney Int*. 2007;72(3):328–336.
12. Masyuk TV, et al. Defects in cholangiocyte fibrocystin expression and ciliary structure in the PCK rat. *Gastroenterology*. 2003;125(5):1303–1310.
13. Xu C, et al. Human ADPKD primary cyst epithelial cells with a novel, single codon deletion in the PKD1 gene exhibit defective ciliary polycystin localization and loss of flow-induced Ca2+ signaling. *Am J Physiol Renal Physiol*. 2007;292(3):F930–F945.
14. Nauli SM, et al. Polycystins 1 and 2 mediate mechanosensation in the primary cilium of kidney cells. *Nat Genet*. 2003;33(2):129–137.
15. Kurbegovic A, Cote O, Couillard M, Ward CJ, Harris PC, Trudel M. Pkd1 transgenic mice: adult model of polycystic kidney disease with extrarenal and renal phenotypes. *Hum Mol Genet*. 2010;19(7):1174–1189.
16. Torres VE, Harris PC. Autosomal dominant polycystic kidney disease: the last 3 years. *Kidney Int*. 2009;76(2):149–168.
17. Yoder BK, Hou X, Guay-Woodford LM. The polycystic kidney disease proteins, polycystin-1, polycystin-2, polaris, and cystin, are co-localized in renal cilia. *J Am Soc Nephrol*. 2002;13(10):2508–2516.
18. Qian F, Germino FJ, Cai Y, Zhang X, Somlo S, Germino GG. PKD1 interacts with PKD2 through a probable coiled-coil domain. *Nat Genet*. 1997;16(2):179–183.
19. Pazour GJ, San Agustin JT, Follit JA, Rosenbaum JL, Witman GB. Polycystin-2 localizes to kidney cilia and the ciliary level is elevated in orpk mice with polycystic kidney disease. *Curr Biol*. 2002;12(11):R378–380.
20. Hanaoka K, et al. Co-assembly of polycystin-1 and -2 produces unique cation-permeable currents. *Nature*. 2000;408(6815):990–994.
21. Hogan MC, et al. Characterization of PKD protein-positive exosome-like vesicles. *J Am Soc Nephrol*. 2009;20(2):278–288.
22. Pisitkun T, Shen RF, Knepper MA. Identification and proteomic profiling of exosomes in human urine. *Proc Natl Acad Sci U S A*. 2004;101(36):13368–13373.
23. Sharif-Naeini R, et al. Polycystin-1 and -2 dosage regulates pressure sensing. *Cell*. 2009;139(3):587–596.
24. Steigelman KA, et al. Polycystin-1 is required for stereocilia structure but not for mechanotransduction in inner ear hair cells. *J Neurosci*. 2011;31(34):12241–12250.
25. Bataille S, et al. Association of PKD2 (polycystin 2) mutations with left-right laterality defects. *Am J Kidney Dis*. 2011;58(3):456–460.
26. Battini L, et al. Loss of polycystin-1 causes centrosome amplification and genomic instability. *Hum Mol Genet*. 2008;17(18):2819–2833.
27. Yamaguchi T, Wallace DP, Magenheimer BS, Hempson SJ, Grantham JJ, Calvet JP. Calcium restriction allows cAMP activation of the B-Raf/ERK pathway, switching cells to a cAMP-dependent growth-stimulated phenotype. *J Biol Chem*. 2004;279(39):40419–40430.
28. Torres VE, Harris PC. Mechanisms of Disease: autosomal dominant and recessive polycystic kidney diseases. *Nat Clin Pract Nephrol*. 2006;2(1):40–55.
29. Vujic M, et al. Incompletely penetrant PKD1 alleles mimic the renal manifestations of ARPKD. *J Am Soc Nephrol*. 2010;21(7):1097–1102.
30. Baert L. Hereditary polycystic kidney disease (adult form): a microdissection study of two cases at an early stage of the disease. *Kidney Int*. 1978;13(6):519–525.
31. Higashihara E, et al. Tolvaptan in autosomal dominant polycystic kidney disease: three years' experience. *Clin J Am Soc Nephrol*. 2011;6(10):2499–2507.
32. Torres VE, et al. Effective treatment of an orthologous model of autosomal dominant polycystic kidney disease. *Nat Med*. 2004;10(4):363–364.
33. Wilson PD. Mouse models of polycystic kidney disease. *Curr Top Dev Biol*. 2008;84:311–350.
34. Lu W, et al. Late onset of renal and hepatic cysts in Pkd1-targeted heterozygotes. *Nat Genet*. 1999;21(2):160–161.
35. Lu W, et al. Perinatal lethality with kidney and pancreas defects in mice with a targetted Pkd1 mutation. *Nat Genet*. 1997;17(2):179–181.
36. Lantinga-van Leeuwen IS, Leonhard WN, van der Wal A, Breuning MH, de Heer E, Peters DJ. Kidney-specific inactivation of the Pkd1 gene induces rapid cyst formation in developing kidneys and a slow onset of disease in adult mice. *Hum Mol Genet*.

2007;16(24):3188–3196.
37. Piontek K, Menezes LF, Garcia-Gonzalez MA, Huso DL, Germino GG. A critical developmental switch defines the kinetics of kidney cyst formation after loss of Pkd1. *Nat Med*. 2007;13(12):1490–1495.
38. Takakura A, Contrino L, Beck AW, Zhou J. Pkd1 inactivation induced in adulthood produces focal cystic disease. *J Am Soc Nephrol*. 2008;19(12):2351–2363.
39. Starremans PG, et al. A mouse model for polycystic kidney disease through a somatic in-frame deletion in the 5' end of Pkd1. *Kidney Int*. 2008; 73(12):1394–1405.
40. Jiang ST, et al. Defining a link with autosomal-dominant polycystic kidney disease in mice with congenitally low expression of Pkd1. *Am J Pathol*. 2006;168(1):205–220.
41. Lantinga-van Leeuwen IS, et al. Lowering of Pkd1 expression is sufficient to cause polycystic kidney disease. *Hum Mol Genet*. 2004;13(24):3069–3077.
42. Hateboer N, et al. Comparison of phenotypes of polycystic kidney disease types 1 and 2. *Lancet*. 1999;353(9147):103–107.
43. Zerres K, Rudnik-Schoneborn S, Deget F. Childhood onset autosomal dominant polycystic kidney disease in sibs: clinical picture and recurrence risk. German Working Group on Paediatric Nephrology (Arbeitsgemeinschaft fuer Padiatrische Nephrologie). *J Med Genet*. 1993;30(7):583–588.
44. Bergmann C, Bruchle NO, Frank V, Rehder H, Zerres K. Perinatal deaths in a family with autosomal dominant polycystic kidney disease and a PKD2 mutation. *N Engl J Med*. 2008;359(3):318–319.
45. Consugar MB, et al. Characterization of large rearrangements in autosomal dominant polycystic kidney disease and the PKD1/TSC2 contiguous gene syndrome. *Kidney Int*. 2008;74(11):1468–1479.
46. Sampson JR, et al. Renal cystic disease in tuberous sclerosis: role of the polycystic kidney disease 1 gene. *Am J Hum Genet*. 1997;61(4):843–851.
47. Brook-Carter PT, et al. Deletion of the TSC2 and PKD1 genes associated with severe infantile polycystic kidney disease--a contiguous gene syndrome. *Nat Genet*. 1994;8(4):328–332.
48. Pei Y, et al. Bilineal disease and trans-heterozygotes in autosomal dominant polycystic kidney disease. *Am J Hum Genet*. 2001;68(2):355–363.
49. Connor A, et al. Mosaicism in autosomal dominant polycystic kidney disease revealed by genetic testing to enable living related renal transplantation. *Am J Transplant*. 2008;8(1):232–237.
50. Harris PC. What is the role of somatic mutation in autosomal dominant polycystic kidney disease? *J Am Soc Nephrol*. 2010;21(7):1073–1076.
51. Muto S, et al. Pioglitazone improves the phenotype and molecular defects of a targeted Pkd1 mutant. *Hum Mol Genet*. 2002;11(15):1731–1742.
52. Paterson AD, Wang KR, Lupea D, St George-Hyslop P, Pei Y. Recurrent fetal loss associated with bilineal inheritance of type 1 autosomal dominant polycystic kidney disease. *Am J Kidney Dis*. 2002;40(1):16–20.
53. Brasier JL, Henske EP. Loss of the polycystic kidney disease (PKD1) region of chromosome 16p13 in renal cyst cells supports a loss-of-function model for cyst pathogenesis. *J Clin Invest*. 1997;99(2):194–199.
54. Qian F, Watnick TJ, Onuchic LF, Germino GG. The molecular basis of focal cyst formation in human autosomal dominant polycystic kidney disease type I. *Cell*. 1996;87(6):979–987.
55. Pei Y, et al. Somatic PKD2 mutations in individual kidney and liver cysts support a "two-hit" model of cystogenesis in type 2 autosomal dominant polycystic kidney disease. *J Am Soc Nephrol*. 1999;10(7):1524–1529.
56. Koptides M, Hadjimichael C, Koupepidou P, Pierides A, Constantinou Deltas C. Germinal and somatic mutations in the PKD2 gene of renal cysts in autosomal dominant polycystic kidney disease. *Hum Mol Genet*. 1999;8(3):509–513.
57. Wu G, et al. Somatic inactivation of Pkd2 results in polycystic kidney disease. *Cell*. 1998;93(2):177–188.
58. Kim I, et al. Polycystin-2 expression is regulated by a PC2-binding domain in the intracellular portion of fibrocystin. *J Biol Chem*. 2008;283(46):31559–31566.
59. Rossetti S, et al. Incompletely penetrant PKD1 alleles suggest a role for gene dosage in cyst initiation in polycystic kidney disease. *Kidney Int*. 2009;75(8):848–855.
60. Pei Y, et al. A missense mutation in PKD1 attenuates the severity of renal disease. *Kidney Int*. 2012;4(4):412–417.
61. Losekoot M, et al. Neonatal onset autosomal dominant polycystic kidney disease (ADPKD) in a patient homozygous for a PKD2 missense mutation due to uniparental disomy. *J Med Genet*. 2012;49(1):37–40.
62. Bergmann C, et al. Mutations in multiple PKD genes may explain early and severe polycystic kidney disease. *J Am Soc Nephrol*. 2011;22(11):2047–2056.
63. Liu P, Jenkins NA, Copeland NG. A highly efficient recombineering-based method for generating conditional knockout mutations. *Genome Res*. 2003;13(3):476–484.
64. Ishikawa I, Saito Y. Volume changes in autosomal dominant polycystic kidneys after the initiation of hemodialysis. *Nephron*. 1993;65(4):649–650.
65. Norman J. Fibrosis and progression of autosomal dominant polycystic kidney disease (ADPKD). *Biochim Biophys Acta*. 2011;1812(10):1327–1336.
66. Gattone VH. Inhibition of renal cystic disease development and progression by a vasopressin V2 receptor antagonist. *Nat Med*. 2003;9(10):1323–1326.
67. Smith LA, et al. Development of polycystic kidney disease in juvenile cystic kidney mice: insights into pathogenesis, ciliary abnormalities, and common features with human disease. *J Am Soc Nephrol*. 2006;17(10):2821–2831.
68. Mazzaccara C, et al. Age-related reference intervals of the main biochemical and hematological parameters in C57BL/6J, 129SV/EV and C3H/HeJ mouse strains. *PLoS One*. 2008;3(11):e3772.
69. Bae KT, et al. Magnetic resonance imaging evaluation of hepatic cysts in early autosomal-dominant polycystic kidney disease: the Consortium for Radiologic Imaging Studies of Polycystic Kidney Disease cohort. *Clin J Am Soc Nephrol*. 2006;1(1):64–69.
70. Reeders ST, et al. Prenatal diagnosis of autosomal dominant polycystic kidney disease with a DNA probe. *Lancet*. 1986;2(8497):6–8.
71. Xiao Z, Zhang S, Cao L, Qiu N, David V, Quarles LD. Conditional disruption of Pkd1 in osteoblasts results in osteopenia due to direct impairment of bone formation. *J Biol Chem*. 2010;285(2):1177–1187.
72. Boulter C, Mulroy S, Webb S, Fleming S, Brindle K, Sandford R. Cardiovascular, skeletal, and renal defects in mice with a targeted disruption of the Pkd1 gene. *Proc Natl Acad Sci U S A*. 2001; 98(21):12174–12179.
73. Chapman AB, Johnson AM, Rainguet S, Hossack K, Gabow P, Schrier RW. Left ventricular hypertrophy in autosomal dominant polycystic kidney disease. *J Am Soc Nephrol*. 1997;8(8):1292–1297.
74. Ishikawa I, Horiguchi T, Shikura N. Lectin peroxidase conjugate reactivity in acquired cystic disease of the kidney. *Nephron*. 1989;51(2):211–214.
75. Vandeursen H, Van Damme B, Baert J, Baert L. Acquired cystic disease of the kidney analyzed by microdissection. *J Urol*. 1991;146(4):1168–1172.
76. Nakanishi K, Sweeney WE Jr, Zerres K, Guay-Woodford LM, Avner ED. Proximal tubular cysts in fetal human autosomal recessive polycystic kidney disease. *J Am Soc Nephrol*. 2000;11(4):760–763.
77. Ahrabi AK, et al. Glomerular and proximal tubule cysts as early manifestations of Pkd1 deletion. *Nephrol Dial Transplant*. 2010;25(4):1067–1078.
78. Wang X, Wu Y, Ward CJ, Harris PC, Torres VE. Vasopressin directly regulates cyst growth in polycystic kidney disease. *J Am Soc Nephrol*. 2008;19(1):102–108.
79. Stroope A, et al. Hepato-renal pathology in Pkd2$^{ws25/-}$ mice, an animal model of autosomal dominant polycystic kidney disease. *Am J Pathol*. 2010;176(3):1282–1291.
80. Besschetnova TY, Kolpakova-Hart E, Guan Y, Zhou J, Olsen BR, Shah JV. Identification of signaling pathways regulating primary cilium length and flow-mediated adaptation. *Curr Biol*. 2010;20(2):182–187.
81. Xu C, et al. Attenuated, flow-induced ATP release contributes to absence of flow-sensitive, purinergic Cai2+ signaling in human ADPKD cyst epithelial cells. *Am J Physiol Renal Physiol*. 2009;296(6):F1464–F1476.
82. Hughes J, et al. The polycystic kidney disease 1 (PKD1) gene encodes a novel protein with multiple cell recognition domains. *Nat Genet*. 1995; 10(2):151–160.
83. Qian F, et al. Cleavage of polycystin-1 requires the receptor for egg jelly domain and is disrupted by human autosomal-dominant polycystic kidney disease 1-associated mutations. *Proc Natl Acad Sci U S A*. 2002;99(26):16981–16986.
84. Newby LJ, Streets AJ, Zhao Y, Harris PC, Ward CJ, Ong AC. Identification, characterization, and localization of a novel kidney polycystin-1-polycystin-2 complex. *J Biol Chem*. 2002;277(23):20763–20773.
85. Vagin O, Kraut JA, Sachs G. Role of N-glycosylation in trafficking of apical membrane proteins in epithelia. *Am J Physiol Renal Physiol*. 2009; 296(3):F459–F469.
86. Wang X, Koulov AV, Kellner WA, Riordan JR, Balch WE. Chemical and biological folding contribute to temperature-sensitive DeltaF508 CFTR trafficking. *Traffic*. 2008;9(11):1878–1893.
87. Liu M, et al. Genetic variation of DKK3 may modify renal disease severity in ADPKD. *J Am Soc Nephrol*. 2010;21(9):1510–1520.
88. Harris PC, et al. Cyst number but not the rate of cystic growth is associated with the mutated gene in autosomal dominant polycystic kidney disease. *J Am Soc Nephrol*. 2006;17(11):3013–3019.
89. Rossetti S, Harris PC. Genotype-phenotype correlations in autosomal dominant and autosomal recessive polycystic kidney disease. *J Am Soc Nephrol*. 2007;18(5):1374–1380.
90. Wang E, et al. Progressive renal distortion by multiple cysts in transgenic mice expressing artificial microRNAs against Pkd1. *J Pathol*. 2010; 222(3):238–248.
91. Li D, et al. The roles of two novel FBN1 gene mutations in the genotype-phenotype correlations of Marfan syndrome and ectopia lentis patients with marfanoid habitus. *Genet Test*. 2008;12(2):325–330.
92. Pereira R, Halford K, Sokolov BP, Khillan JS, Prockop DJ. Phenotypic variability and incomplete penetrance of spontaneous fractures in an inbred strain of transgenic mice expressing a mutated collagen gene (COL1A1). *J Clin Invest*. 1994;93(4):1765–1769.
93. Nadasdy T, Lajoie G, Laszik Z, Blick KE, Molnar-Nadasdy G, Silva FG. Cell proliferation in the developing human kidney. *Pediatr Dev Pathol*. 1998;1(1):49–55.
94. Nadasdy T, Laszik Z, Blick KE, Johnson LD, Silva FG. Proliferative activity of intrinsic cell populations in the normal human kidney. *J Am Soc Nephrol*. 1994;4(12):2032–2039.
95. Grantham JJ, Cook LT, Wetzel LH, Cadnapaphornchai MA, Bae KT. Evidence of extraordinary growth in the progressive enlargement of renal cysts. *Clin J Am Soc Nephrol*. 2010;5(5):889–896.
96. Bastos AP, et al. Pkd1 haploinsufficiency increases renal damage and induces microcyst formation following ischemia/reperfusion. *J Am Soc Nephrol*. 2009;20(11):2389–2402.
97. Nishio S, et al. Pkd1 regulates immortalized proliferation of renal tubular epithelial cells through

p53 induction and JNK activation. *J Clin Invest*. 2005;115(4):910–918.
98. Raj A, Rifkin SA, Andersen E, van Oudenaarden A. Variability in gene expression underlies incomplete penetrance. *Nature*. 2010;463(7283):913–918.
99. Verghese E, Weidenfeld R, Bertram JF, Ricardo SD, Deane JA. Renal cilia display length alterations following tubular injury and are present early in epithelial repair. *Nephrol Dial Transplant*. 2008;23(3):834–841.
100. Wann AK, Knight MM. Primary cilia elongation in response to interleukin-1 mediates the inflammatory response. *Cell Mol Life Sci*. 2012;69(17):2967–2977.
101. Grantham JJ, et al. Volume progression in polycystic kidney disease. *N Engl J Med*. 2006; 354(20):2122–2130.
102. Fedeles SV, et al. A genetic interaction network of five genes for human polycystic kidney and liver diseases defines polycystin-1 as the central determinant of cyst formation. *Nat Genet*. 2011;43(7):639–647.
103. Zode GS, et al. Reduction of ER stress via a chemical chaperone prevents disease phenotypes in a mouse model of primary open angle glaucoma. *J Clin Invest*. 2011;121(9):3542–3553.
104. Bakeberg JL, et al. Epitope-Tagged Pkhd1 tracks the processing, secretion, and localization of fibrocystin. *J Am Soc Nephrol*. 2011;22(12):2266–2277.
105. Xu H, Shen J, Walker CL, Kleymenova E. Tissue-specific expression and splicing of the rat polycystic kidney disease 1 gene. *DNA Seq*. 2001;12(5–6):361–366.
106. Zhang W, et al. Inhibition of tumor growth progression by antiandrogens and mTOR inhibitor in a Pten-deficient mouse model of prostate cancer. *Cancer Res*. 2009;69(18):7466–7472.
107. Fukudome H. A combined SEM and TEM study on the basal labyrinth of the collecting duct in the rat kidney. *Arch Histol Cytol*. 2001;64(3):339–351.
108. Nims N, Vassmer D, Maser RL. Transmembrane domain analysis of polycystin-1, the product of the polycystic kidney disease-1 (PKD1) gene: evidence for 11 membrane-spanning domains. *Biochemistry*. 2003;42(44):13035–13048.